The yeast endocytic early/sorting compartment exists as an independent sub-compartment within the *trans*-Golgi network

Authors

Junko Y. Toshima[1,2]*, Ayana Tsukahara[2], Makoto Nagano[2], Takuro Tojima[3], Daria E. Siekhaus[4], Akihiko Nakano[3], and Jiro Toshima[2]*

Affiliations

[1]School of Health Science, Tokyo University of Technology, 5-23-22 Nishikamata, Ota-ku, Tokyo 144-8535, Japan

[2]Department of Biological Science and Technology, Tokyo University of Science, 6-3-1 Niijyuku, Katsushika-ku, Tokyo 125-8585, Japan

[3]Live Cell Super-Resolution Imaging Research Team, RIKEN Center for Advanced Photonics, Wako, Saitama 351-0198, Japan

[4]Institute of Science and Technology Austria, Am Campus 1, A-3400 Klosterneuburg, Austria

*Corresponding authors:

Telephone 81-3-5876-1501, Fax 81-3-5876-1464, email jtosiscb@rs.tus.ac.jp

Telephone 81-3-6424-2106, Fax 81-3-6424-2112, email toshimajk@stf.teu.ac.jp

Running title: Yeast early/sorting compartment within the TGN

Abstract

Although budding yeast has been extensively used as a model organism for studying organelle functions and intracellular vesicle trafficking, whether it possesses an independent endocytic early/sorting compartment that sorts endocytic cargos to the endo-lysosomal pathway or the recycling pathway has long been unclear. The structure and properties of the endocytic early/sorting compartment differ significantly between organisms; in plant cells the *trans*-Golgi network (TGN) serves this role, whereas in mammalian cells a separate intracellular structure performs this function. The yeast syntaxin homolog Tlg2p, widely localizing to the TGN and endosomal compartments, is presumed to act as a Q-SNARE for endocytic vesicles, but which compartment is the direct target for endocytic vesicles remained unanswered. Here we demonstrate by high-speed and high-resolution 4D imaging of fluorescently labeled endocytic cargos that the Tlg2p-residing compartment within the TGN functions as the early/sorting compartment. After arriving here, endocytic cargos are recycled to the plasma membrane or transported to the yeast Rab5-residing endosomal compartment through the pathway requiring the clathrin adaptors GGAs. Interestingly, Gga2p predominantly localizes at the Tlg2p-residing compartment, and the deletion of GGAs has little effect on another TGN region where Sec7p is present but suppresses dynamics of the Tlg2-residing early/sorting compartment, indicating that the Tlg2p- and Sec7p-residing regions are discrete entities in the mutant. Thus, the Tlg2p-residing region seems to serve as an early/sorting compartment, and function independently of the Sec7p-residing region within the TGN.

Introduction

Clathrin-mediated endocytosis is the best-characterized type of endocytosis in eukaryotic cells and plays crucial roles in many physiological processes (Kaksonen and Roux, 2018; Mettlen et al., 2018). After leaving from the plasma membrane (PM), a clathrin-coated vesicle (CCV) is uncoated and transported to the early/sorting compartment (Cullen and Steinberg, 2018; Valencia et al., 2016). In yeast the molecular mechanisms regulating this CCV formation and internalization have been well characterized, but it still remains unclear how and where uncoated endocytic vesicles are delivered to the early/sorting compartment. A recent study has reported that budding yeast lacks distinct early endosomes and that the Sec7p-residing TGN is the first destination for endocytic traffic, functioning as an early endosome-like compartment (Day et al., 2018). However, several other reports have indicated that yeast has two distinct types of endosomal compartments, one containing yeast Rab5 (Vps21p) and the other containing yeast Rab7 (Lachmann et al., 2012). Additionally, we have previously demonstrated that endocytosed cargos are rarely transported to the Sec7p-residing TGN compartment (Toshima et al., 2014). These inconsistent observations are likely attributable to technical difficulties in visualizing the cargo-sorting process, and have complicated our understanding of the properties of the yeast early/sorting compartment.

The yeast R-SNAREs (soluble N-ethylmaleimide-sensitive factor attachment protein receptors), Snc1p and Snc2p, are yeast orthologs of vesicle-associated membrane protein (VAMP), and were originally identified as proteins required for the fusion of secretory vesicles with the PM via Q-SNAREs Sso1p and Sso2p (Gerst et al.,

1992; Protopopov et al., 1993). Snc1p contains a conserved endocytosis signal, which is recognized by the clathrin adaptor protein and is thereby endocytosed with the CCV (Grote et al., 2000; Gurunathan et al., 2000). Disruption of this endocytic signal causes defects in the internalization of Snc1p itself and other endocytic cargos, such as the fluorescent endocytic tracer FM4-64 and the α-factor receptor Ste2p (Gurunathan et al., 2000). This result suggests that Snc1p and Snc2p function as R-SNAREs in endocytic pathways by interacting with Q-SNAREs. Tlg1p and Tlg2p have high homology to syntaxins, and bind Snc1p and Snc2p (Abeliovich et al., 1998; Holthuis et al., 1998a; Paumet et al., 2001). Since these Q-SNAREs are localized to the TGN and putative early endosomes, these proteins have been considered to play a role in transport between the TGN and endosomal compartments (Holthuis et al., 1998b; Lewis et al., 2000). Tlg1p and Tlg2p are also known to co-localize with endocytosed FM4-64 soon after internalization (Abeliovich et al., 1998; Dobzinski et al., 2015). From these observations, it has been suggested that Tlg1p and/or Tlg2p are Q-SNAREs mediating fusion between endocytic vesicles and early endosomal compartments.

Recent studies using high-speed, high-resolution, and four-dimensional (4D) time-lapse imaging have revealed that in yeast intra-Golgi cargo trafficking from the early Golgi to the TGN is mediated by cisternal maturation (Kurokawa et al., 2019; Losev et al., 2006; Matsuura-Tokita et al., 2006). Detailed localization analyses of various Golgi/TGN-resident proteins have shown that the Golgi-TGN transition gradually proceeds with sequential recruitment of these proteins (Tojima et al., 2019). In this process, Tlg2p appears at the TGN earlier than Sec7p, a marker of the

88 early-to-late TGN, and also disappears before Sec7p from the TGN (Tojima et al.,
89 2019). This observation suggests that endocytic vesicles containing Snc1p R-SNARE
90 might target the TGN compartment where Tlg2p resides although this has not yet been
91 proven directly.

92 In our previous study, we demonstrated that fluorescently labeled endocytic
93 cargo, yeast mating pheromone α-factor (Alexa-α-factor), accumulates at clathrin
94 -coated pits, and is internalized with the CCV (Toshima et al., 2006). Within 5 min after
95 Alexa-α-factor internalization, Alexa-α-factor-labeled endosomal compartments
96 become co-localized with the yeast Rab5, Vps21p, and fuse with each other, resulting in
97 the formation of enlarged endosomal compartments (Toshima et al., 2014). However it
98 has been unclear whether Alexa-α-factor is directly transported to the Vps21p-residing
99 compartment from the endocytic vesicle. We recently showed that although endocytosis
100 is not essential, post-Golgi vesicle transport is crucial for Vps21p-mediated endosome
101 formation (Nagano et al., 2019). Thus, as the TGN seems to play a key role in endocytic
102 cargo transport, it is important to clarify how the TGN regulates endocytic cargo
103 transport to the Vps21p-residing compartment. Here we succeeded in simultaneous
104 triple-color and 4D (3D plus time) observation to visualize endocytic cargo together
105 with the Tlg2p-residing region by super-resolution confocal live imaging microscopy
106 (SCLIM) (Kurokawa and Nakano, 2020; Tojima et al., 2022). We show that
107 Alexa-α-factor endocytosed by the CCV is incorporated directly into the Tlg2p-residing
108 sub-compartment within the TGN, and then moves on from there when another
109 TGN-representative protein Sec7p appears. Such visualization along with genetic

110 manipulations of endocytic pathway components suggest that the Tlg2p-residing
111 sub-compartment within the TGN is the primary endocytic accepting region that serves
112 as an early/sorting compartment that sorts endocytosed cargo to further destinations.
113
114

Results

Endocytosed α-factor is transported to the Tlg2p-residing sub-compartment within the TGN

Sec7p, one of the yeast guanine-nucleotide exchange factors (GEFs) for Arf GTPases, is known as a representative TGN marker (Casler et al., 2021; Kurokawa et al., 2019). A previous study has reported that the Sec7p-residing TGN compartment is the first destination for endocytic traffic and functions as an early endosome-like sorting compartment (Day et al., 2018). However, since Tlg2p, which is a putative Q-SNARE for the endocytic vesicle (Abeliovich et al., 1998; Paumet et al., 2001; Seron et al., 1998) exhibits temporal localization patterns distinct from Sec7p (Tojima et al., 2019), the exact timing and locus of endocytic vesicle targeting remained ambiguous. As a first step towards clarifying this, we compared the localization of Alexa594-labeled α-factor (A594-α-factor) with Tlg2p and Sec7p. The yeast Golgi and TGN are a highly dynamic organelles whose cisternae rapidly change their composition with an approximate maturation rate of less than 1 min (Matsuura-Tokita et al., 2006; Tojima et al., 2019). Therefore, we defined "overlapping" as a distance of less than 129 nm (2 pixels) between two peaks of GFP and mCherry/Alexa594 intensity in 2D imaging. At 5 min after internalization, A594-α-factor began to accumulate at several intracellular puncta, although the majority still remained on the PM (Fig. 1A). GFP-fused Tlg2p was detected in several non-uniform structures, such as puncta or tubules, with different sizes and shapes (Fig. 1, A and F), and ~71% of them clearly overlapped with A594-α-factor-labeled puncta at 5 min after A594-α-factor internalization (Fig. 1B).

After 10 min, A594-α-factor-labeled puncta had increased in both number and fluorescent intensity, and ~77.7% of GFP-Tlg2p overlapped with them (Fig. 1, A and B). In contrast, Sec7-GFP, which was also detected as several punctate structures, did not show significant overlap with A594-α-factor signals either at 5 min (26.0±9.4%) or 10 min (22.7±6.0%) after A594-α-factor internalization (Fig. 1B; Fig. S1A). After 20 min, the number of A594-α-factor-labeled puncta decreased as the α-factor was transported to the vacuole via the pre-vacuolar compartments (PVC) (Toshima et al., 2014) (Fig. 1A). At this time point, most of the A594-α-factor was localized at the puncta around the vacuole and vacuole, and substantial GFP-Tlg2p was also localized at these puncta labeled by A594-α-factor (47.7±3.9%), whereas Sec7-GFP was rarely localized there (5.0±5.4%) (Fig. 1, A and B; Fig. S1A). These observations suggest the localization of GFP-Tlg2p at the early-to-late stage endosomes, as well as the TGN. We also compared the localization of A594-α-factor with Tlg1p, another putative Q-SNARE for the endocytic vesicle, that is reported to localize mainly at the early endosomes and partially at the TGN (Holthuis et al., 1998a). Similar to GFP-Tlg2p, GFP-Tlg1p highly overlapped with A594-α-factor-labeled puncta (74.4±5.9%) at 5 min after A594-α-factor internalization (Fig. 1B and Fig. S1B). However, after 10 min the fraction of A594-α-factor overlapping with GFP-Tlg1p decreased to ~51.1%, and further decreased to ~26.1% after 20 min (Fig. 1B and Fig. S1B). GFP-Tlg1p signals overlapped well with mCherry-Tlg2p-labeled puncta, except at puncta around the vacuole (Fig. S1C), suggesting that Tlg1p localizes at the TGN and early-stage endosomes, as described previously (Holthuis et al., 1998a). To confirm that α-factor

159 overlaps with both Tlg1p and Tlg2p at the TGN just after internalization, we conducted
160 triple color imaging with GFP-Tlg1p, mCherry-Tlg2p, and Alexa647-labeled α-factor
161 (A647-α-factor). As expected, the majority of endocytosed A647-α-factor localized at
162 the compartments where both Tlg1p and Tlg2p are present at 5 min after internalization
163 (Fig. S1D). These observations suggest that α-factor is transported to a region distinct
164 from the Sec7p-residing TGN compartment where Tlg1p and Tlg2p localize, and then
165 from there moves to the PVC via the endocytic pathway.

166 A recent study has demonstrated that the timing of Tlg2p recruitment to the
167 TGN is earlier than that of Sec7p (Tojima et al., 2019). To examine whether Tlg2p
168 localizes at a separate region from the Sec7p-residing region within the TGN, we
169 performed simultaneous dual-color 3D analysis of these proteins using SCLIM. As
170 shown in Figure 1C, we observed two types of GFP-Tlg2p localization, one at regions
171 in which only GFP-Tlg2p was visible, and the other at locations adjacent to the
172 Sec7p-residing region. Previous studies have reported that Tlg2p cycles between late
173 Golgi and endosomal compartments, and thus localizes to both compartments (Lewis et
174 al., 2000). It has also been shown that at the TGN Tlg2p appears earlier than Sec7p, and
175 also disappears before Sec7p from the TGN (Tojima et al., 2019). Therefore, we
176 considered the structures where only GFP-Tlg2p localized to be either an endosomal
177 compartment or the TGN compartment before Sec7-mCherry came in. Localization of
178 GFP-Tlg2p and Sec7-mCherry at the TGN was analyzed by line scan using the xy, xz,
179 or yz planes, which revealed that GFP-Tlg2p signal partially overlaps with the TGN
180 compartment labeled by Sec7-mCherry, but is mostly spatially separated (Fig. 1D;

Video 1). This observation suggests that the Tlg2p-residing structure exists as a sub-compartment that is distinct from the Sec7p-residing structure within the TGN (hereafter referred to as Tlg2p or Sec7p sub-compartment, respectively). We next performed simultaneous triple-color 3D imaging to determine whether α-factor localized to the Tlg2p or the Sec7p sub-compartment. For triple-color imaging with GFP-Tlg2p and Sec7-iRFP, we labeled α-factor with pHrode Red (pHrode-α-factor), whose fluorescent wavelength can be separated from those of GFP and iRFP. pHrode-α-factor clearly labeled endocytic compartments after internalization to the same extent as A594-α-factor (Fig. 1E). 3D SCLIM imaging, similar to the 2D analysis, revealed that at 5 min after internalization pHrode-α-factor signals overlapped with the GFP-Tlg2p signals, around half of which were adjacent to Sec7-iRFP-labeled regions (Fig. 1E). Line scan analyses revealed that the peak of pHrode-α-factor signal coincides with that of GFP-Tlg2p signal rather than Sec7p (Fig. 1F; Video 1). To further understand the spatiotemporal relationship between the Tlg2p and Sec7p sub-compartments during α-factor transport, we performed 4D (3D plus time) imaging by SCLIM. Consistent with the previous study (Tojima et al., 2019), we observed that Sec7-iRFP appeared in the vicinity of GFP-Tlg2p, and then the signal of GFP-Tlg2p gradually disappeared, while that of Sec7-iRFP increased (Fig. 1G; Video 2). During this process, pHrodo-α-factor became joined to the pre-existing Tlg2p sub-compartment and stayed there for several tens of seconds, and then disappeared soon after Sec7-iRFP arrival (Fig. 1G; Video 2). Magnified images from the time series shown in Figure 1G indicate that pHrodo-α-factor already co-localizes with GFP-Tlg2p at the time when

Sec7p shows up (Fig. 1H). This observation suggests that the Tlg2p sub-compartment adjacent to the Sec7p sub-compartment plays a specific role in the endocytic pathway.

Endocytic vesicles interact directly with the Tlg2p-residing sub-compartment

Co-localization of α-factor with the Tlg2p sub-compartment at the early stage of endocytosis motivated us to examine if the Tlg2p sub-compartment is a direct target of endocytic vesicles. We had shown previously that endocytic vesicles labeled with the endocytic vesicle markers Sla1- or Abp1-GFP, moved to the A594-α-factor-labeled compartment, which is considered to be the early endosome (Toshima et al., 2006). Our current simultaneous dual-color 2D imaging showed that when Abp1-mCherry-labeled vesicles began moving, they traveled to Tlg2p sub-compartments and disappeared after arrival there (Fig. 2A; Video 3) We then utilized the *arp3-D11A* mutant, which shows a delay in endocytic vesicle formation and a severe defect in vesicle internalization (Martin et al., 2005), to examine whether we could observe any Tlg2p sub-compartments approaching the endocytic site when endocytic vesicle movement is blocked. As described previously, in the *arp3-D11A* mutant Abp1p's lifetime was remarkably extended, indicating that the formation and internalization of endocytic vesicles were also severely impaired (Fig. 2B; Video 3). Similar to the previous findings obtained when A594-α-factor was used as an early endosome marker (Toshima et al., 2006), the Tlg2p sub-compartment was observed to approach and make contact with the Abp1-mCherry-labeled vesicle remaining on the PM, and then disappeared (Fig. 2B; Video 3).

To further examine the contact between endocytic vesicles and the Tlg2p sub-compartment, we performed dual-color 4D observation by SCLIM. As shown in Figures 2C and 2D, we found that several Abp1-mCherry patches attach to the Tlg2p sub-compartment in both wild-type cells and those from the *arp3-D11A* mutant. Time-laps imaging of a wild type cell revealed that an Abp1-mCherry-labeled endocytic vesicle appeared, stayed for 3-6 sec around the Tlg2p sub-compartment, and then disappeared (Fig. 2E; Video 4). In contrast, in the *arp3-D11A* mutant, an Abp1-mCherry-labeled vesicle stayed around the Tlg2p sub-compartment more than 10 sec and then disappeared (Fig. 2F; Video 5). Because the temporal resolution of SCLIM is 3 sec in this observation, we were unable to track all the Abp1-mCherry signals until their disappearance. The timing of dissociation of Abp1p from the endocytic vesicles depends on the speed of actin depolymerization around the vesicle (Toret et al., 2008) and thus is not constant: some Abp1p signals disappear after reaching the Tlg2p sub-compartment, but others disappear before. Despite this, we observed similar dynamics in at least 18% of Abp1-mCherry-labeled vesicles internalized in wild-type cells (Fig. 2H). We also utilized Vps21p as a marker of another endosomal compartment. In contrast to the Tlg2p sub-compartment, GFP-Vps21-labeled endosomal compartments often fused with each other, forming larger structures, and Abp1-mCherry-labeled vesicles rarely coalesced into them (Fig. 2, G and H). To further test if the Tlg2p sub-compartment interacting with Abp1-mCherry-labeled vesicles was within the TGN, we performed triple-color 4D imaging including Sec7-iRFP and found that the Abp1-mCherry-labeled vesicle stayed and disappeared on the Tlg2p

sub-compartment adjacent to the Sec7p sub-compartment (Fig. 2, I and J). These results support the idea that the initial destination of endocytic vesicles is the Tlg2p sub-compartment.

α-factor transported to the Tlg2p sub-compartment moves to the Vps21p-residing endosome, together with Tlg2p

We previously demonstrated that Vps21p localizes predominantly at endosomal compartments (Toshima et al., 2014). Co-localization between A594-α-factor and GFP-Tlg2p at the early-to-late stage of the endocytic pathway prompted us to investigate whether Vps21p also localizes to the Tlg2p sub-compartment. To this end, we imaged GFP-Tlg2p and mCherry-Vps21p simultaneously by 2D epi-fluorescence microscopy, and found that ~53% of GFP-Tlg2p signals overlaps with mCherry-Vps21p (Fig. 3, A and B). This overlapping localization was observed at the Vps21p-residing smaller structures (Fig. 3A, white arrow heads) and the larger Tlg2p sub-compartments (Fig. 3A, yellow arrow heads). We also found that ~26% of the Sec7-mCherry-labeled sub-compartment overlapped with GFP-Vps21p signals, suggesting that Vps21p partially localizes around the TGN as well as in endosomal compartments. Interestingly, we observed that mCherry-Vps21p-labeled vesicles associate with and move around the Tlg2p sub-compartment over 10 seconds, and line scan analyses revealed that the Vps21p signal well overlaps with the GFP-Tlg2p signal (Fig. 3C). Triple-color 3D imaging demonstrated that mCherry-Vps21p signals often made contact with the Tlg2p

sub-compartment adjacent to the Sec7p sub-compartment (Fig. 3, D and E; Video 6). This interaction seemed to be transient because mCherry-Vps21p attached to the Tlg2p sub-compartment for several tens of seconds and then became detached from there (Fig. 3F; Video 6). Additionally, we observed that small GFP-Tlg2p signals moved together with mCherry-Vps21p when the mCherry-Vps21p-labeled puncta detached from the Tlg2p sub-compartment (Fig. 3G; Video 6). Thus, the Vps21p-residing structures appear to transiently contact the Tlg2p sub-compartment, transporting Tlg2p to the Vps21p-residing compartment.

We next conducted 2D imaging using GFP-Tlg2p, mCherry-Vps21p and A647-α-factor to determine the order of α-factor delivery. At 5-20 min after internalization, the rate of A647-α-factor overlapping with GFP-Tlg2p and/or mCherry-Vps21p changed in a time-dependent manner (Fig. 3, H and I). We conducted quantitative analysis, categorizing A647-α-factor localization as overlapping with Tlg2p only (α-factor and Tlg2p), with Vps21p only (α-factor and Vps21p), with both of them (α-factor & Tlg2p & Vps21p), or as α-factor alone. This revealed that the overlap of α-factor signals with GFP-Tlg2p was highest at 5 min and then gradually decreased from 10 to 20 min, whereas that with mCherry-Vps21p increased from 5 to 20 min (Fig. 3, H and I). This result suggested that α-factor transported to the Tlg2p sub-compartment moves to the Vps21p-residing compartment in the endocytic pathway. At 15 min after internalization, α-factor mostly reached the PVC (Toshima et al., 2014), and at the same time a portion of the GFP-Tlg2p signals was still co-localized with A647-α-factor and mCherry-Vps21p (Fig. 3H), suggesting that Tlg2p exits the TGN

and is then transported to the PVC via the Vps21p-residing compartment. To confirm this, we examined if Tlg2p accumulates in endosomal intermediates observed in the mutant lacking the yeast Rab5 paralogs, *VPS21* and *YPT52* (Toshima et al., 2014). As shown previously, A594-α-factor accumulated in multiple endosomal intermediates in the *vps21*Δ *ypt52*Δ mutant, and Tlg2p was well localized there (Fig. 3, J and K). It is noteworthy that the number of Tlg2p puncta increased (Fig. 3J) while that of Sec7p puncta did not change in the mutant (Toshima et al., 2014). These observations support the idea that Tlg2p is transported to the PVC via the Vps21p-residing compartment.

GGA adaptors are required for transport of endocytic cargo from the Tlg2p sub-compartment to the Vps21p-residing compartment

A previous study has reported that after reaching the TGN, α-factor is transported to the PVC, dependent on the TGN-resident Golgi-associated, γ-adaptin ear containing, Arf binding protein (GGA) adaptors, Gga1p and Gga2p (Day et al., 2018). GGA adaptors were also shown to mediate TGN-to endosome traffic (Black and Pelham, 2000). Therefore, we speculated that deletion of *GGA1* and *GGA2* might cause accumulation of α-factor at the TGN compartment where α-factor is located. In agreement with previous observations, endocytosed A594-α-factor in the *gga1*Δ *gga2*Δ mutant accumulated at several puncta in the cytoplasm at 20 min after internalization, whereas in wild-type cells it was mostly transported to the vacuole at this time (Fig. 4A). Accumulation of A594-α-factor was also observed in cells lacking epsin-related Ent3p/5p (Nagano et al., 2019), but not observed in cells lacking Apl4p, a subunit of the

313 AP-1 complex (Fig. 4A), indicating that the AP-1-dependent pathway is not essential
314 for sorting of α-factor to the vacuole. By comparing the localization of A594-α-factor
315 with the Sec7-GFP-labeled sub-compartment, we found that the regions where
316 A594-α-factor accumulated differed between the mutants (Fig. 4B). In the
317 *gga1*Δ *gga2*Δ mutant, localization of Sec7-GFP overlapping with A594-α-factor at this
318 resolution (< 130 nm) was markedly increased to 55.7±5.8%, whereas it was only
319 slightly increased in the *ent3*Δ *ent5*Δ mutant (11.7±4.1%), relative to that in wild-type
320 cells (2.6±2.3%) at 20 min after A594-α-factor internalization (Fig. 4, B and C). These
321 results indicate a requirement for GGA adaptors in the export of A594-α-factor from
322 the regions near the Sec7-GFP-labeled TGN compartment.

323 Since A594-α-factor is first transported to the Tlg2p sub-compartment, we
324 speculated that A594-α-factor might accumulate at the region distinct from the Sec7p
325 sub-compartment in the *gga1*Δ *gga2*Δ mutant. Thus, we examined the temporal changes
326 in A594-α-factor localization in the *gga1*Δ *gga2*Δ mutant by comparing the localization
327 with GFP-Tlg2p. In contrast to wild-type cells, in the *gga1*Δ *gga2*Δ mutant, the overlap
328 between A594-α-factor and GFP-Tlg2p increased over time (Fig. 4, D and E). We
329 further classified the distance between the two peaks into those <65 nm (1 pixel) and
330 those from 65-130 nm (1-2 pixels), and found that more than half of the α-factor
331 accumulated at sites neighboring the GFP-Tlg2p peak (1-2 pixel) (33.5±11.8%,
332 34.5±9.0%, 57.0±15.3%, and 51.1±10.2% at 5, 10, 20, and 40 min, respectively) (Fig.
333 4E). To examine α-factor localization with higher spatial resolution, we observed the
334 localization of pHrode-α-factor and GFP-Tlg2p at the Golgi/TGN by dual-color 3D

335 SCLIM. Similar to images observed by 2D epi-fluorescence microscopy, we found that
336 α-factor accumulates at the Tlg2p-residing region and its adjacent region (Fig. 4, F-H).
337 Furthermore, triple-color 3D imaging demonstrated that pHrode-α-factor signal mostly
338 co-localized with GFP-Tlg2 rather than Sec7-iRFP (Fig. 4, I and J; Video 7). These
339 results suggest that in the *gga1*Δ *gga2*Δ mutant α-factor accumulates in or around Tlg2p
340 sub-compartments due to the defective transport out of the compartment.
341
342 **GGA adaptors are required for turnover of the Tlg2p sub-compartment**
343 GGA adaptors have been believed to function at the Sec7p-residing TGN
344 compartment (Daboussi et al., 2012; Dell'Angelica et al., 2000) but our finding that
345 α-factor accumulates at the Tlg2p sub-compartment in the *gga1*Δ *gga2*Δ mutant
346 suggests that GGA may be required for the transport from the Tlg2p sub-compartment
347 instead of the Sec7p sub-compartment. Thus, we next investigated the effects of
348 deleting *GGA1* and *GGA2* on the Tlg2p or Sec7p sub-compartment. Simultaneous
349 dual-color 2D imaging revealed that in the *gga1*Δ *gga2*Δ mutant the Tlg2p and Sec7p
350 sub-compartments were more segregated and that the overlap of GFP-Tlg2p with
351 Sec7-mCherry was markedly decreased (46.3±2.6%), relative to wild-type cells
352 (76.9±7.7%) (Fig. 5, A and B). The double-color 4D SCLIM observation demonstrated
353 that Sec7-mCherry signals appeared in the vicinity of the pre-existing Tlg2p
354 sub-compartment and then Tlg2p disappeared gradually consistent with the previous
355 report in wild-type cells (Fig. 5, C and D; Video 8) (Tojima et al., 2019). In contrast, in
356 the *gga1*Δ *gga2*Δ mutant, the Sec7p sub-compartment turned over, whereas the turnover

of the Tlg2p sub-compartment was significantly delayed, resulting in an increase of the sub-compartments displaying only GFP-Tlg2p (Fig. 5, E-G; Video 9). Line scan analyses revealed that Tlg2p and Sec7p sub-compartments were clearly segregated in the *gga1*Δ *gga2*Δ mutant (Fig. 5, H and I; Video 10). We also examined the localization of Tlg1p and found that it shows similar dynamics to Tlg2p in both wild-type and the *gga1*Δ *gga2*Δ cells (Fig. S2, A-D). These results suggest that the Tlg2p and Sec7p sub-compartments are discrete entities in the mutant.

Since GGA adaptors are required for the turnover of the Tlg2p sub-compartment, we speculate that the adaptors play a role there. Our simultaneous dual-color 2D imaging showed that ~64.6% of Gga2p signals overlapped with the Tlg2p sub-compartment (Fig. S3A). To examine the spatiotemporal localization of Gga2p precisely, we performed triple-color imaging of GFP-Tlg2p, Sec7-iRFP, and Gga2-mCherry by SCLIM. As reported previously, we observed that Gga2p appears around the Sec7p sub-compartment and disappears at a similar time as Sec7p (Fig. 5, J-K; Video 11) (Daboussi et al., 2012; Tojima et al., 2019). As expected, a comparison of the spatiotemporal localization of Gga2p, Tlg2p, and Sec7p in the Golgi/TGN revealed that Gga2-mCherry signals co-localize with GFP-Tlg2p-residing sub-compartments (Fig. 5K; Video 11). We also found that the Gga2-mCherry signal remained after the GFP-Tlg2p signal disappeared, but the Gga2-mCherry-labeled region seemed to be distinct from Sec7-iRFP-labeled sub-compartment (Fig. 5L; Video 11). Thus, Gga2p likely appears at the Tlg2p sub-compartment during the decay phase of Tlg2p, and mediates the transport of α-factor and presumably Tlg2p itself from the

379 Tlg2p sub-compartment to the Vps21p-residing endosomal compartment.

380

381 **Endocytosed Snc1p is recycled back to the PM via the Tlg2p sub-compartment**

382 Previous studies have shown that Snc1p, a putative endocytic R-SNARE,
383 transiently localizes to the Sec7p sub-compartment after being endocytosed, and returns
384 to the cell surface through the secretory pathway (Best et al., 2020; Robinson et al.,
385 2006). We have demonstrated in the present study that the Tlg2p sub-compartment is
386 the first destination for endocytic traffic, and that endocytic cargo is transported to the
387 Vps21p-residing compartment without passing through the Sec7p sub-compartment.
388 Thus, we next wished to determine whether the pathway back to the PM is also
389 mediated through the Tlg2p sub-compartments. We first confirmed that GFP-Snc1p and
390 A594-α-factor are loaded into the same endocytic vesicle. Using total internal reflection
391 fluorescence microscopy (TIRFM), we observed that A594-α-factor and GFP-Snc1p
392 were localized in the same vesicles and moved together in the vicinity of the PM surface
393 in wild-type cells (Fig. 6A). As reported previously (Black and Pelham, 2000), in the
394 *gga1*Δ *gga2*Δ mutant, GFP-Snc1p accumulated at intracellular structures (Fig. S3B),
395 suggesting that the transport of GFP-Snc1p to the PM, as well as that of endocytic cargo
396 to the vacuole, is impaired. We found that the intracellular localization of GFP-Snc1p
397 overlapped well with the Tlg2p sub-compartment in both wild-type (73.2±12.4%) and
398 *gga1*Δ *gga2*Δ mutant cells (78.0±11.4%) (Fig. S3C), suggesting that GFP-Snc1p is
399 sorted to the PM through the Tlg2p sub-compartment.

400 We then wished to determine which sub-compartment, the Tlg2p-residing or

401 the Sec7p-residing, mediates Snc1p transport form the TGN to the PM. Simultaneous
402 triple-color observation by SCLIM showed that mCherry-Snc1p mostly localized to the
403 sub-compartment in which GFP-Tlg2p was present (Fig. 6B). Line scan analyses
404 showed that peaks of mCherry-Snc1p and GFP-Tlg2p signal are almost coincident, but
405 that the peak of Sec7-iRFP signal is slightly apart from them (Fig. 6C). Interestingly,
406 4D SCLIM imaging demonstrated that the mCherry-Snc1p signal remained in the
407 compartment from which GFP-Tlg2p departed and then disappeared at the same time as
408 or slightly earlier than Sec7-iRFP (Fig. 6D). This observation suggests that Tlg2p and
409 Snc1p are both sorted to this compartment, but then transported by distinct trafficking
410 pathways with different timings. The compartment in which Snc1p remains after Tlg2p
411 leaves appeared to be distinct from the Sec7p sub-compartment (Fig. 6E). We next
412 confirmed the localization of Snc1p using the *gga1*Δ *gga2*Δ mutant, because in the
413 *gga1*Δ *gga2*Δ mutant the Tlg2p and Sec7p sub-compartments were more clearly
414 segregated (Fig. 5, E-I). As expected, mCherry-Snc1p signals did not co-localize with
415 Sec7-mCherry but clearly co-localized with GFP-Tlg2p signals (Fig. 6, F and G; Video
416 12). Time-lapse imaging showed that mCherry-Snc1p signals were also persistent with
417 GFP-Tlg2 signals after the disappearance of Sec7-iRFP (Fig. 6H). To further confirm
418 that the Tlg2p sub-compartment is an early/sorting compartment, we utilized mutant
419 lacking the *RCY1* gene, because Rcy1p, a F-box protein, has been shown to be required
420 for the transport of Snc1p to the PM (Galan et al., 2001; Ma and Burd, 2020;
421 Wiederkehr et al., 2000). Previous studies have demonstrated that in the *rcy1*Δ mutant
422 Snc1p partially co-localizes with Tlg1p but does not co-localize with Sec7p (Best et al.,

2020; Ma and Burd, 2019). Similar to the case of Tlg1p, 3D SCLIM imaging demonstrated that mCherry-Snc1p signals overlap mainly with the Tlg2p sub-compartment adjacent to the Sec7p sub-compartment in the mutant (Fig. 6I; Video 13). These results clearly indicate that endocytosed Snc1p is sorted to the PM via the Tlg2p sub-compartment, and taken together with the results obtained from assays using fluorescently labeled α-factor, suggest that the Tlg2p-residing region serves as the endocytic early/sorting compartment.

Discussion

The Tlg2p sub-compartment functions as an endocytic early/sorting compartment

On the basis of the data presented here and in previous studies, we propose a role for the Tlg2p sub-compartment as an early/sorting compartment in the endocytic pathway (Fig. 7). In contrast to the previous observation (Day et al., 2018), we have shown here that endocytic cargo is incorporated into a Tlg2p sub-compartment distinct from the Sec7p-residing one at the TGN. Then, the endocytic cargo α-factor is transported to the Vps21p-residing compartment dependent on GGA adaptors although whether they directly bind to the cargo is unclear, while Snc1p is transported to the PM. A recent study demonstrated that in plants the TGN has at least two subregions (zones) responsible for secretory and vacuolar trafficking (Nakano, 2022; Shimizu et al., 2021), and endocytic cargo transport via the Tlg2p sub-compartment might mediate this later zone. We recently reported that Vps9p, a GEF for Vps21p, is recruited to the TGN, and then transported to the endosome to activate Vps21p through Ent3p/5p-mediated vesicle transport (Nagano et al., 2019). Previous studies reported that GGA adaptors-enriched vesicles include Ent3p and Ent5p (Daboussi et al., 2012), and thus Vps9p might be recruited to and transported from the Tlg2p sub-compartment. In *ent3*Δ *ent5*Δ cells as well as *vps21*Δ *ypt52*Δ cells, Vps21p-mediated endosomal transport is impaired (Nagano et al., 2019), and thus α-factor and Tlg2p presumably accumulate at the Vps21p-residing compartment. In contrast, deletion of Gga1p/2p has a negligible effect on Vps21p-mediated endosome formation (Nagano et al., 2019), but affects turnover of the Tlg2p sub-compartment (Fig. 7).

453

454 **Integrating the present model with earlier observations**

455 The yeast Q-SNAREs Tlg1p and Tlg2p were first identified a few decades
456 ago, and their roles have been debated because of their localization at the TGN and
457 endosomal compartment (Abeliovich et al., 1998; Holthuis et al., 1998b; Seron et al.,
458 1998). Previous studies using electron microscopy showed that endocytic cargo is first
459 transported to the tubular/vesicular structure that contains Tlg1p after internalization
460 (Prescianotto-Baschong and Riezman, 1998). A recent study by Day et al reported that
461 both Tlg1p and Tlg2p shows substantial colocalization with Sec7p (~50%
462 GFP-Tlg1p-labeled puncta overlap with Sec7p-residing TGN), but rarely overlap with
463 Vps8-residing PVC (Day et al., 2018). Holthuis et al. reported that upon subcellular
464 fractionation the two proteins peaked at different densities, leading the authors to
465 propose that the two proteins are found in a putative early endosome, and the
466 Golgi/PVC respectively (Holthuis et al., 1998b). However, their distribution within the
467 fractions entirely overlapped and Tlg2p is also found in the peak fraction of Tlg1p
468 (Holthuis et al., 1998b). Matching these observations, we observed that both Tlg1p and
469 Tlg2p substantially localize at the TGN while Tlg1p localizes at the PVC less than
470 Tlg2p. Thus, Tlg1p seems to localize at the Tlg2p sub-compartment and function
471 together with it.

472 By examining the localization, we demonstrated that Alexa-α-factor,
473 transported to the Tlg2p sub-compartment adjacent to the Sec7p sub-compartment,
474 moves to the Vps21p-residing compartment presumably together with Tlg2p. As Tlg2p

interacts with Snc2p, a potential endocytic R-SNARE, and its deletion caused a defect in the endocytic pathway (Abeliovich et al., 1998; Paumet et al., 2001; Seron et al., 1998), the primary role of Tlg2p in the endocytic pathway seems to be in mediating fusion of the endocytic vesicle with the early/sorting compartment. Additionally, Tlg2p present in the Vps21p-residing compartment might have a role in endosomal fusion. After being transported to the Vps21p-residing compartment, Tlg2p may be returned to the early/sorting compartment by interacting with Ypt6p (yeast Rab6) and the Golgi-associated retrograde protein (GARP) complex (Siniossoglou and Pelham, 2001; Suda et al., 2013).

Tojima et al. have previously demonstrated that Tlg2p and Sec7p overlap during Golgi/TGN maturation (Tojima et al., 2019), and Day et al. have reported that FM4-64 and α-factor is transported to the Sec7p sub-compartment immediately after endocytic internalization (Day et al., 2018). Our present analysis indicates that Tlg2p partially overlaps with Sec7p, although the major part of the Tlg2p sub-compartment exists separate from the Sec7p-residing one. The clathrin-residing region has also been shown to segregate from the Tlg2p sub-compartment, although it largely overlaps with the Sec7p sub-compartment (Tojima et al., 2019), supporting the idea that the Tlg2p and Sec7p sub-compartments are segregated spatially. Our model, therefore, is not inconsistent with those built on previous observations, but adds the concept that the Tlg2p-residing region, rather than the Sec7p-residing region, functions as an endocytic early/sorting compartment.

Possible mechanism for early/sorting compartment generation

How the endocytic early/sorting compartment is generated and turned over has been unclear both in plants and mammals. Our findings provide a new insight into the mechanism. Recent studies have demonstrated that the appearance and the dynamic behaviors of Golgi/TGN-resident proteins exhibit a unique order of events during Golgi/TGN maturation (Kim et al., 2016; Kurokawa et al., 2019; Thomas et al., 2021; Tojima et al., 2019). Tojima et al. proposed that the Golgi/TGN maturation process can be classified into three successive stages: the Golgi stage, the early TGN stage, and the late TGN stage; Tlg2p was categorized as an early TGN-resident protein (Tojima et al., 2019). Our present results indicate that, after capturing endocytic vesicles, the Tlg2p sub-compartment gradually disappears through export of Tlg2p to the Vps21p-residing compartment. The Tlg2p sub-compartment is presumably regenerated by Sys1p-mediated retrograde transport. Sys1p, a late Golgi-resident protein, recruits GARP complexes through the Sys1-Arl3-Arl1-Imh1 cascade (Graham, 2004), and interacts with vesicles containing Tlg1p derived from endosomes (Chen et al., 2019; Siniossoglou and Pelham, 2001). Tlg1p is known to bind directly to the GARP complex and mediates the retrograde transport from the late endosome (Siniossoglou and Pelham, 2001). Tlg2p has been also reported to be cycled between the TGN and endosome (Lewis et al., 2000). Interestingly, a previous study reported that the majority of the Sys1p-residing compartment is not accompanied by clathrin appearance (Tojima et al., 2019), suggesting that Sys1p resides in a distinct compartment from the Sec7p-residing one. The observation that the Sys1p-residing compartment appears before Tlg2p and

519 matures into the Tlg2p-residing one (Tojima et al., 2019) supports the idea that Sys1p
520 may play a role in generating the early/sorting compartment.
521
522 **Role of GGA adaptors in endocytic cargo transport**
523 A previous study has suggested the importance of GGA adaptors in the export
524 of α-factor from the Sec7p sub-compartment (Day et al., 2018). Black and Pelham
525 reported that Pep12p, a yeast syntaxin localized primarily at the late endosome, is also
526 mislocalized to the Tlg1p high-density membranes in *gga1*Δ *gga2*Δ cell, and suggested
527 that an aberrant early endosome structure may cause a defect in the TGN-to-endosome
528 traffic (Black and Pelham, 2000). Here we have shown that in *gga1*Δ *gga2*Δ cells
529 α-factor accumulates at the Tlg2p sub-compartment. Interestingly, in *gga1*Δ *gga2*Δ
530 cells, turnover of the Tlg2p- and Tlg1p-residing sub-compartment is impaired, and these
531 observations suggest that export of cargos by GGA adaptors is important for normal
532 turnover of the Tlg2p sub-compartment. As GGA adaptors are reported to bind directly
533 to ubiquitin, which function as a sorting signal for lysosomal degradation (Scott et al.,
534 2004), the ubiquitination signal could mediate the export of α-factor from the Tlg2p
535 sub-compartment. Several cell-surface proteins, including the α-factor receptor Ste3p,
536 are known to be ubiquitinated, thereby being sorted from the TGN to the vacuole
537 (Buelto et al., 2020; Scott et al., 2004). The α-factor receptor Ste2p is also ubiquitinated
538 upon ligand binding, promoting incorporation of the α-factor-Ste2p complex into the
539 clathrin-coated vesicle (Hicke and Riezman, 1996; Toshima et al., 2009). Thus, after
540 being transported to the Tlg2p sub-compartment, the ubiquitinated α-factor-Ste2p

complex could be exported to the Vps21p-residing compartment by binding to GGA adaptors.

Two major clathrin adaptors, GGA adaptors and the AP-1 complex, were implicated to act in TGN-endosome trafficking (Traub, 2005). Daboussi et al. showed that the major population of Gga2p and AP-1 is separated both temporally and spatially, and that Gga2p arrives earlier than AP-1 at almost the same time point as Sec7p (Daboussi et al., 2012). In contrast, Gga1p appears to arrive at the TGN earlier than Gga2p, presumably with similar timing to Tlg2p because it arrives 3 sec earlier than Chs5p, a component of the exomer complex (Anton-Plagaro et al., 2021). A recent study has reported that GGA adaptors, but not the AP-1 complex, are necessary for the transport of newly synthesized vacuolar protein from the TGN to the vacuole via the VPS pathway (Casler and Glick, 2020). We previously demonstrated that convergence of the endocytic and VPS pathways occurs upstream of the requirement for Vps21p in the early stage of the endocytic pathway (Toshima et al., 2014). Taken together, these observations suggest that the endocytic cargo derived from the PM and the biosynthetic cargo for the VPS pathway both reach the Tlg2p sub-compartment and exit there by a GGA-adaptor-dependent mechanism.

Materials and Methods

Yeast strains, growth conditions, and plasmids

The yeast strains used in this study are listed in Table S1. All strains were grown at 25°C in standard rich medium (YPD) or synthetic medium (SM) supplemented with 2% glucose and appropriate amino acids. The N-terminal GFP-tagged Tlg2p was expressed as follows: the SacI and HindIII fragment (containing iGFP-TLG2) extracted from YLplac211-iGFP-TLG2 plasmid (Addgene #105262) was inserted into the SacI and EcoRV-digested pRS303 (pRS303-iGFP-Tlg2). To integrate pRS303-iGFP-TLG2 into the HIS3 locus, the plasmid was linearized by NheI and transformed into wild-type or mutant cells. The N-terminal GFP tagging of Vps21p and the C-terminal fluorescent protein tagging of proteins was performed as described previously (Toshima et al., 2014).

Fluorescence labeling of α-factor and endocytosis assays

Fluorescence labeling of α-factor was performed as described previously[23]. For endocytosis assays, cells were grown to an OD_{600} of ~0.5 in 0.5 ml YPD, briefly centrifuged, and resuspended in 20 μl SM with 5 μM Alexa Fluor-labeled α-factor. After incubation on ice for 2 h, the cells were washed with ice-cold SM. Internalization was initiated by addition of SM containing 4% glucose and amino acids at 25°C.

Fluorescence microscopy and image analysis

2D imaging was performed using an Olympus IX83 microscope equipped with a x100/NA 1.40 (Olympus) or a x100/NA 1.49 (Olympus) objective and Orca-AG cooled CCD camera (Hamamatsu), using Metamorph software (Universal Imaging). For TIRF illumination, optically pumped semiconductor laser (OPSL) (Coherent) with emission of at 488 nm (OBIS 488LS-50) and at 561 nm (OBIS 561LS-50) were used to excite GFP or mCherry/Alexa594, respectively. Simultaneous imaging of red and green fluorescence was performed using an Olympus IX83 microscope, described above, and an image splitter (Dual-View; Optical Insights) that divided the red and green components of the images with a 565-nm dichroic mirror and passed the red component through a 630/50 nm filter and the green component through a 530/30 nm filter. These split signals were taken simultaneously with one CCD camera, described above. 2D triple-color imaging were performed using an Olympus IX81 microscope equipped with a high-speed filter changer (Lambda 10-3; Sutter Instruments) that can change filter sets within 40 ms. All cells were imaged during the early- to mid-logarithmic phase. Images for analysis of co-localization of red and green signals were acquired using simultaneous imaging (64.5 nm pixel size), described above. Intensity profiles of GFP-fused protein and mCherry-fused protein or A594-α-factor were generated using the Plot Profile tool (ImageJ v1.53a) across the center of fluorescence signals. All the data which shows two peaks of GFP and mCherry/Alexa Fluor intensity with a distance of less than 2 pixels, are defined as "overlapping".

3D and 4D imaging were performed with SCLIM (Kurokawa and Nakano, 2020; Tojima et al., 2022). The system is composed of an Olympus IX73 microscope,

601 solid-state lasers with emission at 473 nm (Blues™, 50 mW; Cobolt), 561 nm (Jive™,
602 50 mW; Cobolt) and 671 nm (CL671-100-S, 100 mW; CrystaLaser), a UPlanXApo
603 x100/NA 1.45 (Olympus) objective, a high-speed spinning-disk confocal scanner
604 (Yokogawa Electric), a custom-built piezo actuator (Yokogawa Electric), a custom-built
605 emission splitter unit, image intensifiers (Hamamatsu) with a custom-made cooling
606 system, a magnification lens system to provide x266.7 final magnification, and three
607 EM-CCD cameras (Hamamatsu) for green, red, and infrared fluorescence channels. The
608 pixel size corresponds to 0.06 μm on the sample plane. For 3D observations, we
609 collected 21 optical sections spaced 0.2 μm apart (z-range = 4.0 μm). Z-stack images
610 were reconstructed to 3D images and deconvoluted by using theoretical point spread
611 functions with Volocity (Quorum Technologies).
612
613

Acknowledgements

This work was supported by JSPS KAKENHI GRANT #18K062291, and the Takeda Science Foundation to J.Y.T., as well as JSPS KAKENHI GRANT #19K065710, the Takeda Science Foundation, and Life Science Foundation of JAPAN to J.T.

Author contributions

J.Y. Toshima designed and performed most experiments, analyzed data, and wrote the manuscript. A. Tsukahara performed the initial experiments and analysis. M. Nagano and T. Tojima performed the part of experiments and provided critical input. D.E. Siekhaus and A. Nakano reviewed and edited the manuscript, and provided critical input. J. Toshima designed and supervised the study and wrote and edited the manuscript.

Declaration of interest

The authors declare no competing interests.

631 **References**

632

633 Abeliovich, H., E. Grote, P. Novick, and S. Ferro-Novick. 1998. Tlg2p, a yeast syntaxin
634 homolog that resides on the Golgi and endocytic structures. *Journal of*
635 *Biological Chemistry*. 273:11719-11727.
636 Anton-Plagaro, C., N. Sanchez, R. Valle, J.M. Mulet, M.C. Duncan, and C. Roncero.
637 2021. Exomer complex regulates protein traffic at the TGN through differential
638 interactions with cargos and clathrin adaptor complexes. *FASEB journal :*
639 *official publication of the Federation of American Societies for Experimental*
640 *Biology*. 35:e21615.
641 Best, J.T., P. Xu, J.G. McGuire, S.N. Leahy, and T.R. Graham. 2020. Yeast
642 synaptobrevin, Snc1, engages distinct routes of postendocytic recycling
643 mediated by a sorting nexin, Rcy1-COPI, and retromer. *Mol Biol Cell*.
644 31:944-962.
645 Black, M.W., and H.R. Pelham. 2000. A selective transport route from Golgi to late
646 endosomes that requires the yeast GGA proteins. *J Cell Biol*. 151:587-600.
647 Buelto, D., C.W. Hung, Q.L. Aoh, S. Lahiri, and M.C. Duncan. 2020. Plasma
648 membrane to vacuole traffic induced by glucose starvation requires
649 Gga2-dependent sorting at thetrans-Golgi network. *Biol Cell*. 112:349-367.
650 Casler, J.C., and B.S. Glick. 2020. A microscopy-based kinetic analysis of yeast
651 vacuolar protein sorting. *Elife*. 9:e56844.
652 Casler, J.C., N. Johnson, A.H. Krahn, A. Pantazopoulou, K.J. Day, and B.S. Glick. 2021.
653 Clathrin adaptors mediate two sequential pathways of intra-Golgi recycling.
654 *Journal of Cell Biology*. 221:e202103199.
655 Chen, Y.T., I.H. Wang, Y.H. Wang, W.Y. Chiu, J.H. Hu, W.H. Chen, and F.J.S. Lee.
656 2019. Action of Arl1 GTPase and golgin Imh1 in Ypt6-independent retrograde
657 transport from endosomes to the trans-Golgi network. *Mol Biol Cell*.
658 30:1008-1019.
659 Cullen, P.J., and F. Steinberg. 2018. To degrade or not to degrade: mechanisms and
660 significance of endocytic recycling. *Nat Rev Mol Cell Bio*. 19:679-696.
661 Daboussi, L., G. Costaguta, and G.S. Payne. 2012. Phosphoinositide-mediated clathrin
662 adaptor progression at the trans-Golgi network. *Nat Cell Biol*. 14:239-248.
663 Day, K.J., J.C. Casler, and B.S. Glick. 2018. Budding Yeast Has a Minimal

664 Endomembrane System. *Dev Cell*. 44:56-72e54.
665 Dell'Angelica, E.C., R. Puertollano, C. Mullins, R.C. Aguilar, J.D. Vargas, L.M.
666 Hartnell, and J.S. Bonifacino. 2000. GGAs: A family of ADP ribosylation
667 factor-binding proteins related to adaptors and associated with the Golgi
668 complex. *Journal of Cell Biology*. 149:81-93.
669 Dobzinski, N., S.G. Chuartzman, R. Kama, M. Schuldiner, and J.E. Gerst. 2015.
670 Starvation-Dependent Regulation of Golgi Quality Control Links the TOR
671 Signaling and Vacuolar Protein Sorting Pathways. *Cell Rep*. 12:1876-1886.
672 Galan, J.M., A. Wiederkehr, J.H. Seol, R. Haguenauer-Tsapis, R.J. Deshaies, H.
673 Riezman, and M. Peter. 2001. Skp1p and the F-box protein Rcy1p form a
674 non-SCF complex involved in recycling of the SNARE Snc1p in yeast. *Mol Cell*
675 *Biol*. 21:3105-3117.
676 Gerst, J.E., L. Rodgers, M. Riggs, and M. Wigler. 1992. Snc1, a Yeast Homolog of the
677 Synaptic Vesicle-Associated Membrane-Protein Synaptobrevin Gene Family -
678 Genetic Interactions with the Ras and Cap Genes. *Proc Natl Acad Sci U S A*.
679 89:4338-4342.
680 Graham, T.R. 2004. Membrane targeting: Getting Arl to the Golgi. *Current Biology*.
681 14:R483-R485.
682 Grote, E., G. Vlacich, M. Pypaert, and P.J. Novick. 2000. A snc1 endocytosis mutant:
683 Phenotypic analysis and suppression by overproduction of dihydrosphingosine
684 phosphate lyase. *Mol Biol Cell*. 11:4051-4065.
685 Gurunathan, S., D. Chapman-Shimshoni, S. Trajkovic, and J.E. Gerst. 2000. Yeast
686 exocytic v-SNAREs confer endocytosis. *Mol Biol Cell*. 11:3629-3643.
687 Hicke, L., and H. Riezman. 1996. Ubiquitination of a yeast plasma membrane receptor
688 signals its ligand-stimulated endocytosis. *Cell*. 84:277-287.
689 Holthuis, J.C., B.J. Nichols, and H.R. Pelham. 1998a. The syntaxin Tlg1p mediates
690 trafficking of chitin synthase III to polarized growth sites in yeast. *Mol Biol Cell*.
691 9:3383-3397.
692 Holthuis, J.C.M., B.J. Nichols, S. Dhruvakumar, and H.R.B. Pelham. 1998b. Two
693 syntaxin homologues in the TGN/endosomal system of yeast. *Embo Journal*.
694 17:113-126.
695 Kaksonen, M., and A. Roux. 2018. Mechanisms of clathrin-mediated endocytosis. *Nat*
696 *Rev Mol Cell Bio*. 19:313-326.

697 Kim, J.J., Z. Lipatova, U. Majumdar, and N. Segev. 2016. Regulation of Golgi Cisternal
698 Progression by Ypt/Rab GTPases. *Dev Cell*. 36:440-452.
699 Kurokawa, K., and A. Nakano. 2020. Live-cell Imaging by Super-resolution Confocal
700 Live Imaging Microscopy (SCLIM): Simultaneous Three-color and
701 Four-dimensional Live Cell Imaging with High Space and Time Resolution.
702 *Bio-Protocol*. 10:e3732.
703 Kurokawa, K., H. Osakada, T. Kojidani, M. Waga, Y. Suda, H. Asakawa, T. Haraguchi,
704 and A. Nakano. 2019. Visualization of secretory cargo transport within the
705 Golgi apparatus. *Journal of Cell Biology*. 218:1602-1618.
706 Lachmann, J., F.A. Barr, and C. Ungermann. 2012. The Msb3/Gyp3 GAP controls the
707 activity of the Rab GTPases Vps21 and Ypt7 at endosomes and vacuoles. *Mol*
708 *Biol Cell*. 23:2516-2526.
709 Lewis, M.J., B.J. Nichols, C. Prescianotto-Baschong, H. Riezman, and H.R. Pelham.
710 2000. Specific retrieval of the exocytic SNARE Snc1p from early yeast
711 endosomes. *Mol Biol Cell*. 11:23-38.
712 Losev, E., C.A. Reinke, J. Jellen, D.E. Strongin, B.J. Bevis, and B.S. Glick. 2006. Golgi
713 maturation visualized in living yeast. *Nature*. 441:1002-1006.
714 Ma, M.X., and C.G. Burd. 2019. Retrograde trafficking and quality control of yeast
715 synaptobrevin, Snc1, are conferred by its transmembrane domain. *Mol Biol Cell*.
716 30:1729-1742.
717 Ma, M.X., and C.G. Burd. 2020. Retrograde trafficking and plasma membrane recycling
718 pathways of the budding yeast Saccharomyces cerevisiae. *Traffic*. 21:45-59.
719 Martin, A.C., X.P. Xu, I. Rouiller, M. Kaksonen, Y. Sun, L. Belmont, N. Volkmann, D.
720 Hanein, M. Welch, and D.G. Drubin. 2005. Effects of Arp2 and Arp3
721 nucleotide-binding pocket mutations on Arp2/3 complex function. *J Cell Biol*.
722 168:315-328.
723 Matsuura-Tokita, K., M. Takeuchi, A. Ichihara, K. Mikuriya, and A. Nakano. 2006.
724 Live imaging of yeast Golgi cisternal maturation. *Nature*. 441:1007-1010.
725 Mettlen, M., P.H. Chen, S. Srinivasan, G. Danuser, and S.L. Schmid. 2018. Regulation
726 of Clathrin-Mediated Endocytosis. *Annual Review of Biochemistry, Vol 87*.
727 87:871-896.
728 Nagano, M., J.Y. Toshima, D.E. Siekhaus, and J. Toshima. 2019. Rab5-mediated
729 endosome formation is regulated at the trans-Golgi network. *Commun Biol*.

730 2:419.
731 Nakano, A. 2022. The Golgi Apparatus and its Next-Door Neighbors. *Frontiers in Cell*
732 *and Developmental Biology*. 10:884360.
733 Paumet, F., B. Brugger, F. Parlati, J.A. McNew, T.H. Sollner, and J.E. Rothman. 2001.
734 A t-SNARE of the endocytic pathway must be activated for fusion. *Journal of*
735 *Cell Biology*. 155:961-968.
736 Prescianotto-Baschong, C., and H. Riezman. 1998. Morphology of the yeast endocytic
737 pathway. *Mol Biol Cell*. 9:173-189.
738 Protopopov, V., B. Govindan, P. Novick, and J.E. Gerst. 1993. Homologs of the
739 Synaptobrevin Vamp Family of Synaptic Vesicle Proteins Function on the Late
740 Secretory Pathway in Saccharomyces-Cerevisiae. *Cell*. 74:855-861.
741 Robinson, M., P.P. Poon, C. Schindler, L.E. Murray, R. Kama, G. Gabriely, R.A. Singer,
742 A. Spang, G.C. Johnston, and J.E. Gerst. 2006. The Gcs1 Arf-GAP mediates
743 Snc1,2 v-SNARE retrieval to the Golgi in yeast. *Mol Biol Cell*. 17:1845-1858.
744 Scott, P.M., P.S. Bilodeau, O. Zhdankina, S.C. Winistorfer, M.J. Hauglund, M.M.
745 Allaman, W.R. Kearney, A.D. Robertson, A.L. Boman, and R.C. Piper. 2004.
746 GGA proteins bind ubiquitin to facilitate sorting at the trans-Golgi network. *Nat*
747 *Cell Biol*. 6:252-259.
748 Seron, K., V. Tieaho, C. Prescianotto-Baschong, T. Aust, M.O. Blondel, P. Guillaud, G.
749 Devilliers, O.W. Rossanese, B.S. Glick, H. Riezman, S. Keranen, and R.
750 Haguenauer-Tsapis. 1998. A yeast t-SNARE involved in endocytosis. *Mol Biol*
751 *Cell*. 9:2873-2889.
752 Shimizu, Y., J. Takagi, E. Ito, Y. Ito, K. Ebine, Y. Komatsu, Y. Goto, M. Sato, K.
753 Toyooka, T. Ueda, K. Kurokawa, T. Uemura, and A. Nakano. 2021. Cargo
754 sorting zones in the trans-Golgi network visualized by super-resolution confocal
755 live imaging microscopy in plants. *Nat Commun*. 12:1901.
756 Siniossoglou, S., and H.R. Pelham. 2001. An effector of Ypt6p binds the SNARE Tlg1p
757 and mediates selective fusion of vesicles with late Golgi membranes. *Embo J*.
758 20:5991-5998.
759 Suda, Y., K. Kurokawa, R. Hirata, and A. Nakano. 2013. Rab GAP cascade regulates
760 dynamics of Ypt6 in the Golgi traffic. *Proc Natl Acad Sci U S A*.
761 110:18976-18981.
762 Thomas, L.L., C.M. Highland, and J.C. Fromme. 2021. Arf1 orchestrates Rab GTPase

763 conversion at the trans-Golgi network. *Mol Biol Cell*. 32:1104-1120.
764 Tojima, T., D. Miyashiro, Y. Kosugi, and A. Nakano. 2022. Super-resolution live
765 imaging ofcargo traffic through the Golgi apparatus in mammalian cells.
766 *Methods Mol Biol*. in press.
767 Tojima, T., Y. Suda, M. Ishii, K. Kurokawa, and A. Nakano. 2019. Spatiotemporal
768 dissection of the trans-Golgi network in budding yeast. *J Cell Sci*.
769 132:jcs231159.
770 Toret, C.P., L. Lee, M. Sekiya-Kawasaki, and D.G. Drubin. 2008. Multiple pathways
771 regulate endocytic coat disassembly in Saccharomyces cerevisiae for optimal
772 downstream trafficking. *Traffic*. 9:848-859.
773 Toshima, J.Y., J.I. Nakanishi, K. Mizuno, J. Toshima, and D.G. Drubin. 2009.
774 Requirements for Recruitment of a G Protein-coupled Receptor to
775 Clathrin-coated Pits in Budding Yeast. *Mol Biol Cell*. 20:5039-5050.
776 Toshima, J.Y., S. Nishinoaki, Y. Sato, W. Yamamoto, D. Furukawa, D.E. Siekhaus, A.
777 Sawaguchi, and J. Toshima. 2014. Bifurcation of the endocytic pathway into
778 Rab5-dependent and -independent transport to the vacuole. *Nat Commun*.
779 5:3498.
780 Toshima, J.Y., J. Toshima, M. Kaksonen, A.C. Martin, D.S. King, and D.G. Drubin.
781 2006. Spatial dynamics of receptor-mediated endocytic trafficking in budding
782 yeast revealed by using fluorescent alpha-factor derivatives. *Proc Natl Acad Sci*
783 *U S A*. 103:5793-5798.
784 Traub, L.M. 2005. Common principles in clathrin-mediated sorting at the Golgi and the
785 plasma membrane. *Bba-Mol Cell Res*. 1744:415-437.
786 Valencia, J.P., K. Goodman, and M.S. Otegui. 2016. Endocytosis and Endosomal
787 Trafficking in Plants. *Annu Rev Plant Biol*. 67:309-335.
788 Wiederkehr, A., S. Avaro, C. Prescianotto-Baschong, R. Haguenauer-Tsapis, and H.
789 Riezman. 2000. The F-box protein Rcy1p is involved in endocytic membrane
790 traffic and recycling out of an early endosome in Saccharomyces cerevisiae. *J*
791 *Cell Biol*. 149:397-410.
792
793

794 **Figure legends**

795 **Figure 1. Localization of endocytosed α-factor at the Tlg2p-residing compartment**

796 (**A**) 2D imaging of A594-α-factor and GFP-Tlg2p. Arrowheads indicate examples of
797 overlapping localization. Representative fluorescence intensity profiles along a line
798 (direction from 'a' to 'b') are indicated in the lower panels. (**B**) Quantification of
799 GFP-Tlg2p, GFP-Tlg1 and Sec7-GFP overlapping with A594-α-factor. Data show the
800 mean ± SEM from n ≥ 3 experiments (n > 30 puncta for each experiment). Different
801 letters indicate significant differences at $P < 0.05$ between the indicated times (i.e., no
802 significant difference for a vs. a, significant difference for a vs. b with $p < 0.05$),
803 one-way ANOVA with Tukey's post-hoc test. Error bars indicate the standard SD from
804 n ≥ 3 experiments (n ≥ 30 puncta for each experiment). (**C**) 3D SCLIM imaging of
805 GFP-Tlg2p and Sec7-mCherry. White dashed lines indicate cell edges. (**D**) Multi-angle
806 magnified 3D views of the boxed area and the representative fluorescence intensity
807 profiles. Line scan as in A shown at right. (**E**) 3D SCLIM imaging of GFP-Tlg2p,
808 Sec7-iRFP and pHrode-α-factor; boxed areas shown magnified in (F-H). The images
809 were acquired simultaneously at 5 min after pHrode-α-factor internalization. (**F**)
810 Multi-angle magnified 3D views of the yellow-boxed area in (E). Line scan as in A
811 shown at right. (**G**) Time series of region in the white-boxed area in (E). Arrows and
812 arrowheads denote the appearance and disappearance of each marker. (**H**)
813 Higher-magnification views of the red-boxed area in (G). Scale bars, 2.5 μm.

814

815 **Figure 2. Dynamic behavior of the Tlg2p-residing compartment, endocytic vesicles,**

816 **and cargos** (**A, B**) 2D imaging of GFP-Tlg2p and Abp1-mCherry in wild-type (A) and
817 *arp3-D11A* cells (B). Kymographs along lines in the upper merged image are shown in
818 the panels below. A time series of the boxed area in (A) and (B) is shown under the
819 kymograph. Arrowheads highlight the movement of Abp1p towards the Tlg2p
820 sub-compartment. (**C-F**) 4D SCLIM imaging of GFP-Tlg2p and Abp1-mCherry in
821 wild-type (C, E) and *arp3-D11A* (D, F). (E, F) Time-series of the areas boxed in (C) and
822 (D) are shown in multi-angle magnified 3D views. White and yellow arrowheads
823 indicate the dynamics of different Abp1p patches. (**G**) 4D SCLIM imaging of
824 GFP-Vps21p and Abp1-mCherry in wild-type cells. Time-series of the boxed areas are
825 shown in the right panels. White and red arrowheads indicate the dynamics of the
826 Vps21p-residing endosome and Abp1p patch. **(H)** The percentages of Abp1p patches
827 that disappeared from the Tlg2p- or Vps21p-residing compartment. Error bars indicate
828 the SD from $n \geq 10$ biological replicates ($n \geq 40$ Abp1p patches for each experiment).
829 $^{***}P < 0.001$, unpaired t-test with Welch's correction. **(I)** 4D SCLIM imaging of
830 wild-type cells expressing GFP-Tlg2p, Sec7-iRFP, and Abp1-mCherry. **(J)** Time-series
831 of the boxed area in (I) are shown in magnified 3D views. Arrowheads indicate the
832 incorporation of Abp1p patches to the sub-compartment including GFP-Tlg2p and
833 Sec7-iRFP signals. Scale bars, 2.5 μm.
834
835 **Figure 3. Alexa-α-factor is transported from the Tlg2p-residing compartment to**
836 **the Vps21p-residing endosomal compartment** (**A**) 2D imaging of GFP-Tlg2p or
837 Sec7-mCherry and mCherry/GFP-Vps21p. (**B**) Quantification of Tlg2p or Sec7p

838 overlapping with Vps21p. Error bars indicate the SD from n ≥ 3 experiments (n ≥ 30
839 puncta for each experiment). (**C**) Time series of the region in the boxed area in (A).
840 Representative fluorescence intensity profiles along a line in the merged image at 8 sec
841 are shown to the right. Yellow arrowhead indicates overlapping localization. (**D**) 4D
842 SCLIM imaging of GFP-Tlg2p, Sec7-iRFP, and mCherry-Vps21p. Arrowheads indicate
843 examples of the association of GFP-Tlg2p and mCherry-Vps21p. (**E**) Magnified views
844 from the time-series in (F). Arrowheads indicate a Vps21p-residing endosome.
845 Representative fluorescence intensity profiles along a line in the merged images at 15
846 sec are shown to the right. (**F**) Time series of the region in the boxed area in (D). (**G**)
847 Further magnified views from the time-series in (F). (**H**) 2D imaging of A647-α-factor,
848 GFP-Tlg2p and mCherry-Vps21p. The images were acquired at 5 and 15 min after
849 A647-α-factor internalization. Higher-magnification views of the boxed areas are
850 shown in the lower panels. (**I**) Quantification of A647-α-factor overlapping with
851 GFP-Tlg2p or mCherry-Vps21p. Data show the mean ± SEM from n ≥ 3 experiments (n
852 > 30 puncta for each experiment). Comparisons are made between the same colors, with
853 different letters indicating significant difference ($P < 0.05$) between the indicated times,
854 one-way ANOVA with Tukey's post-hoc test. (**J**) 2D imaging of A594-α-factor and
855 GFP-Tlg2p in *vps21*Δ *ypt52*Δ cells. The images were acquired at 5 and 20 min after
856 A594-α-factor internalization. Higher-magnification views of the boxed area are shown
857 in the right panels. Arrowheads indicate examples of the overlapping localization of
858 A594-α-factor and GFP-Tlg2p. (**K**) Quantification of GFP-Tlg2p overlapping with
859 A594-α-factor. Error bars indicate the SD from n ≥ 3 experiments (n > 30 puncta for

each experiment). *$P < 0.05$, unpaired t-test with Welch's correction. Scale bars, 2.5 μm.

Figure 4. GGA adaptors are required for export of A594-α-factor out of the Tlg2p-residing compartment (**A**) 2D imaging of A594-α-factor in cells lacking clathrin adaptor proteins. (**B**) 2D imaging of A594-α-factor and Sec7-GFP in cells lacking clathrin adaptor proteins. The images were acquired simultaneously at 20 min after A594-α-factor internalization. Arrowheads indicate examples of overlapping localization. (**C**) Quantification of Sec7-GFP overlapping with A594-α-factor. Error bars indicate the SD from n ≥ 3 experiments (n > 30 puncta for each experiment). ***$P < 0.001$, unpaired t-test with Welch's correction. (**D**) 2D imaging of A594-α-factor and GFP-Tlg2p in *gga1*Δ *gga2*Δ cells. Higher-magnification views of the boxed area are shown in the right panels. Representative fluorescence intensity profiles along lines in the merged images are indicated in the right panels. (**E**) Quantification of GFP-Tlg2p overlapping with A594-α-factor in *gga1*Δ *gga2*Δ cells. The bars surrounded by red lines indicate the total ratio of the Tlg2p sub-compartment overlapping with α-factor. Error bars indicate the SD from n ≥ 3 experiments (n > 30 puncta for each experiment). **(F)** 3D SCLIM imaging of GFP-Tlg2p and pHrode-α-factor in *gga1*Δ *gga2*Δ cells. The images were acquired simultaneously at 20 min after pHrode-α-factor internalization. **(G, H)** Multi-angle magnified 3D views of the boxed areas in (F), representing co-localization (G) or adjacent localization (H) of GFP-Tlg2p and pHrode-α-factor. **(I)** 3D SCLIM imaging of GFP-Tlg2p, Sec7-iRFP and pHrode-α-factor in *gga1*Δ *gga2*Δ

882 cells. The images were acquired simultaneously at 10 min after pHrode-α-factor
883 internalization. **(J)** Multi-angle magnified 3D views of the boxed area in (I). Scale bars,
884 2.5 μm.
885
886 **Figure 5. The transition from the Tlg2p- to the Sec7p-residing compartment**
887 **requires GGA adaptors** (**A**) 2D imaging of GFP-Tlg2p and Sec7-mCherry in
888 *gga1*Δ *gga2*Δ cells. Representative intensity profiles of GFP-Tlg2p or Sec7-mCherry
889 along a line in the merged images are indicated in the right lower panel. (**B**)
890 Quantification of GFP-Tlg2p overlapping with Sec7-mCherry in wild-type and
891 *gga1*Δ *gga2*Δ cells. Error bars indicate the SD from n ≥ 3 experiments (n > 30 puncta
892 for each experiment). $^{**}P < 0.01$, unpaired t-test with Welch's correction. (**C, E**) 4D
893 SCLIM imaging of GFP-Tlg2p and Sec7-mCherry in wild-type cells (C) and
894 *gga1*Δ *gga2*Δ cells (E). The time series of regions in the boxed areas in (C) are shown
895 in the lower panels. Arrows and arrowheads denote the appearance and disappearance
896 of each marker. (**D, G**) Time course changes in relative fluorescence intensity of
897 GFP-Tlg2p and Sec7-mCherry in the boxed areas in (C) or (E). (**F**) Time series of the
898 region in the boxed area in (E). (**H, I**) Multi-angle magnified 3D views from (F). (**J**) 4D
899 SCLIM imaging of GFP-Tlg2p, Gga2-mCherry and Sec7-iRFP. The time series of
900 regions in the boxed areas in (J) are shown in the lower panels. (**K, L**) Multi-angle
901 magnified 3D views of time points from (J). Scale bars, 2.5 μm.
902
903 **Figure 6. Snc1p is sorted to the PM via the Tlg2p-residing compartment** (**A**) TIRF

904 imaging of GFP-Snc1p and A594-α-factor in wild-type cells. The images were acquired
905 simultaneously at 5 min after A594-α-factor internalization. Arrowheads indicate
906 A594-α-factor puncta including GFP-Snc1p. (**B-E**) 4D SCLIM imaging of GFP-Tlg2p,
907 mCherry-Snc1p and Sec7-iRFP in wild-type cells. (C) Multi-angle magnified 3D views
908 from the 70 sec image in (D). Representative fluorescence intensity profiles along lines
909 (direction from 'a' to 'b') in the merged images are indicated in the right panels. **(**D**)**
910 Time series of regions in the boxed area in (B). **(**E**)** Higher-magnification views of the
911 indicated time-points. (**F-H**) 4D SCLIM imaging of GFP-Tlg2p, mCherry-Snc1p and
912 Sec7-iRFP in *gga1*Δ *gga2*Δ cells. (G) Multi-angle magnified 3D views and
913 representative fluorescence intensity profiles at 55 sec in (H). (H) The time series of
914 region in the boxed area in (F). **(I)** 3D SCLIM imaging of GFP-Tlg2p, mCherry-Snc1p,
915 and Sec7-iRFP in *rcy1*Δ cells. Multi-angle magnified 3D views of the boxed area and
916 representative fluorescence intensity profiles shown in the lower panels. Scale bars, 2.5
917 μm.
918
919 **Figure 7. Model showing the role of the Tlg2p-residing compartment as an**
920 **early/sorting compartment in the endocytic pathway.** Schematic showing the
921 Tlg2p-residing area as a discrete early/recycling sub-compartment that sorts endocytic
922 cargo to the endocytic or recycling pathway. The effects of *gga1*Δ *gga2*Δ cells on the
923 post-TGN trafficking pathway are shown on the right. See details in the text.
924
925

926 **Supplemental materials**

927 **Figure S1. Localization of α-factor, Sec7p, Tlg1p, and Tlg2p in wild-type cells.** (**A,**
928 **B**) 2D imaging of A594-α-factor and Sec7-GFP (A) or GFP-Tlg1p (B) in wild type cells.
929 The images were acquired at 5, 10, or 20 min after A594-α-factor internalization.
930 Yellow arrowheads indicate examples of overlapping localization. Red and green
931 arrowheads indicate example of A594-α-factor or GFP signal, respectively.
932 Higher-magnification views of the boxed area are shown in the right panels.
933 Representative fluorescence intensity profiles along a line (direction from 'a' to 'b') in
934 the merged images are indicated in the lower panels. (**C**) 2D imaging of GFP-Tlg1p and
935 mCherry-Tlg2p in wild type cells shown also in DIC at right. Yellow arrowheads
936 indicate examples of overlapping localization. Red arrowheads indicate example of
937 puncta predominantly localizing mCherry-Tlg2p. Higher-magnification views of the
938 boxed area are shown in the right panels. Representative fluorescence intensity profiles
939 along a line (direction from 'a' to 'b') in the merged images are indicated in the lower
940 panels. (D) 2D imaging of A647-α-factor, GFP-Tlg1p and mCherry-Tlg2p. The images
941 were acquired at 5 min after A647-α-factor internalization. Yellow and white
942 arrowheads indicate examples of puncta in which all fluorescent signals overlap. Scale
943 bars, 2.5 μm.
944
945 **Figure S2. Dynamics of Tlg1p and Tlg2p in wild-type and *gga1*Δ *gga2*Δ cells. (A,**
946 **C)** 2D imaging of GFP-Tlg1p and mCherry-Tlg2p in a wild-type (A) or *gga1*Δ *gga2*Δ
947 (C) cell. A time series of the region boxed in (A, C) are shown in the lower panels.

948 Arrows and arrowheads denote the appearance and disappearance of each marker. (**B,**
949 **D**) Time course changes in relative fluorescence intensity of GFP-Tlg1p and
950 mCherry-Tlg2p. Scale bars, 2.5 μm.
951
952 **Figure S3. Localization of Gga2p and Snc1p at the Tlg2p-residing compartment.**
953 (**A**) 2D imaging of GFP-Tlg2p and Gga2-mCherry. Higher-magnification views of the
954 boxed area are shown in the right panels. Representative fluorescence intensity profiles
955 along a line (direction from 'a' to 'b') in the merged images are indicated in the lower
956 panels. Quantification of Gga2-mCherry overlapping with GFP-Tlg2p in wild-type cells
957 is shown in the right panels. (**B**) 2D imaging of GFP-Tlg2p and mCherry-Snc1p in
958 wild-type and *gga1*Δ *gga2*Δ cells. Higher-magnification views of the boxed area are
959 shown in the right panels. Representative fluorescence intensity profiles along a line
960 (direction from 'a' to 'b') in the merged images are indicated in the lower panels.
961 Yellow arrowheads indicate examples of overlapping localization. (**C**) Quantification of
962 Snc1p overlapping with Tlg2p is shown to the right. Error bars indicate the SD from n ≥
963 3 experiments (n > 30 puncta for each experiment).
964

965 **Supplementary Movies**

966 **Video 1**

967 Left; Multi-angle 3D reconstructed movie of GFP-Tlg2p (green) and Sec7-mCherry
968 (red) in wild-type cell. Right; Multi-angle 3D reconstructed movie of GFP-Tlg2p
969 (green), Sec7-iRFP (red) and pHrodo-α-factor (cyan).

970

971 **Video 2**

972 Triple-color 4D movie of GFP-Tlg2p (green), Sec7-iRFP(red) and pHrodo-α-factor
973 (cyan) in a wild-type cell. Arrows indicate examples of the sequential appearance and
974 disappearance of each protein.

975

976 **Video 3**

977 Upper video; 2D time-lapse movie of Abp1-mCherry (red in merge) and GFP-Tlg2p
978 (green in merge) in wild-type cell. Arrows indicate movement of an
979 Abp1-mCherry-labeled endocytic vesicle toward the GFP-Tlg2p-labeled
980 sub-compartment. Lower video; 2D time-lapse movie of Abp1-mCherry (red in merge)
981 and GFP-Tlg2p (green in merge) in the *arp3-D11A* mutant. Arrows indicate movement
982 of the GFP-Tlg2p-labeled sub-compartment toward an Abp1-mCherry-labeled
983 endocytic vesicle.

984

985 **Video 4**

986 Dual-color 4D movie of GFP-Tlg2p (green) and Abp1-mCherry (red) in a wild-type cell.

Arrows indicate examples of Abp1-mCherry-labeled vesicles disappearing on the GFP-Tlg2p-labeled sub-compartment.

Video 5

Dual-color 4D movie of GFP-Tlg2p (green) and Abp1-mCherry (red) in the *arp3-D11A* mutant. Arrows indicate examples of Abp1-mCherry-labeled vesicles disappearing onto the GFP-Tlg2p-residing sub-compartment.

Video 6

Triple-color 4D movie of GFP-Tlg2p (green), mCherry-Vps21p (red) and Sec7-iRFP (cyan) in a wild-type cell. Arrows indicate examples of association between GFP-Tlg2p and mCherry-Vps21p.

Video 7

Multi-angle 3D reconstructed movie of GFP-Tlg2p (green), Sec7-iRFP (red) and pHrodo-α-factor (cyan) in the *gga1*Δ *gga2*Δ mutant.

Video 8

Dual-color 4D movie of GFP-Tlg2p (green) and Sec7-mCherry (red) in wild-type cell. Arrows indicate examples of sequential appearance and disappearance of each protein.

Video 9

Dual-color 4D movie of GFP-Tlg2p (green) and Sec7-mCherry (red) in the *gga1*Δ *gga2*Δ mutant.

Video 10

Multi-angle 3D reconstructed movie of GFP-Tlg2p (green) and Sec7-mCherry (red) in the *gga1*Δ *gga2*Δ mutant.

Video 11

Triple-color 4D movie of GFP-Tlg2p (green), Sec7-iRFP (red) and Gga2-mCherry (cyan) in a wild-type cell. Arrows indicate examples of the sequential appearance and disappearance of each protein.

Video 12

Multi-angle 3D reconstructed movie of GFP-Tlg2p (green), Sec7-iRFP (red) and mCherry-Snc1p (cyan) in the *gga1*Δ *gga2*Δ mutant.

Video 13

Multi-angle 3D reconstructed movie of GFP-Tlg2p (green), Sec7-iRFP (red) and mCherry-Snc1p (cyan) in the *rcy1*Δ mutant.

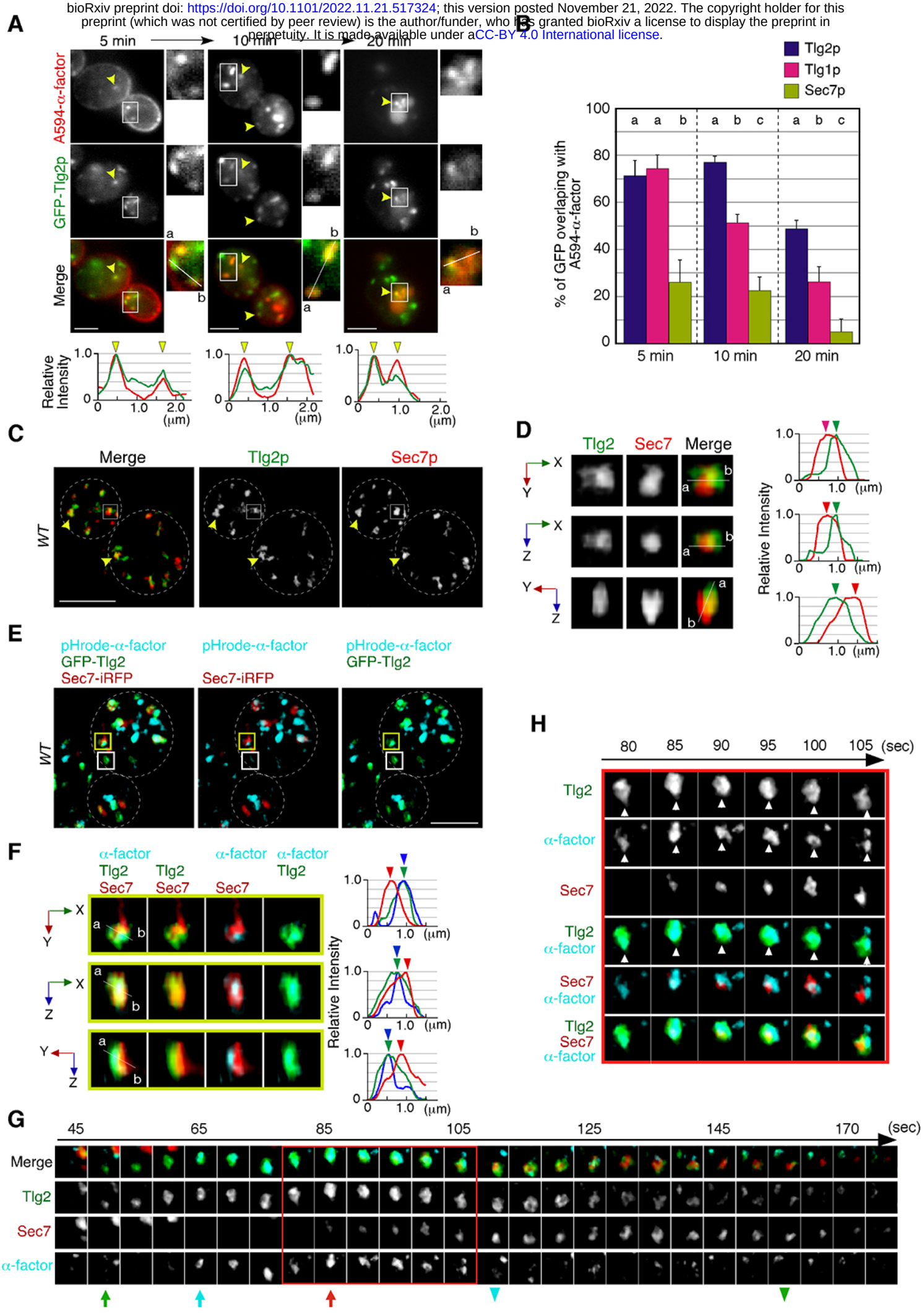

Figure 1. Toshima et al.

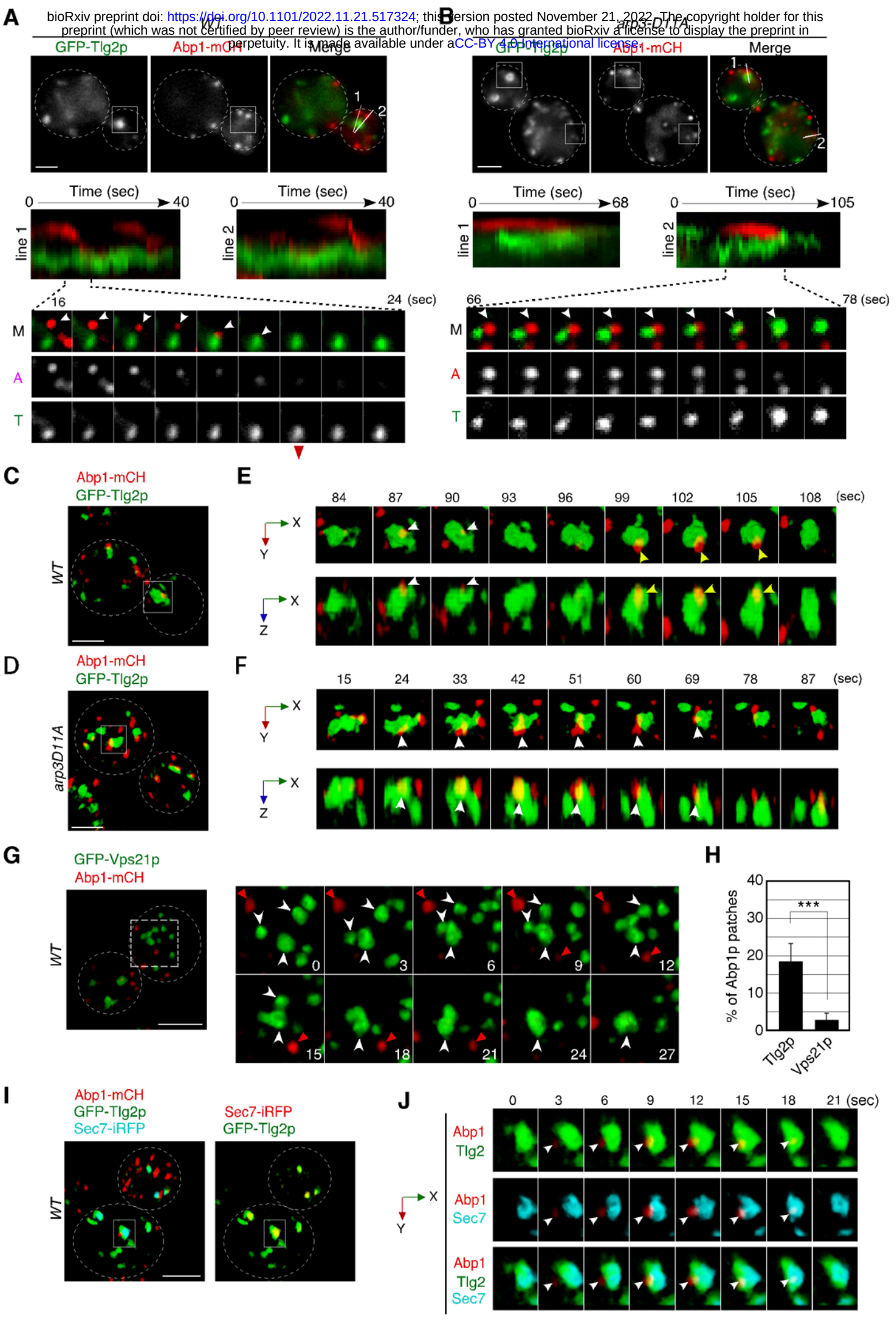

Figure 2. Toshima et al.

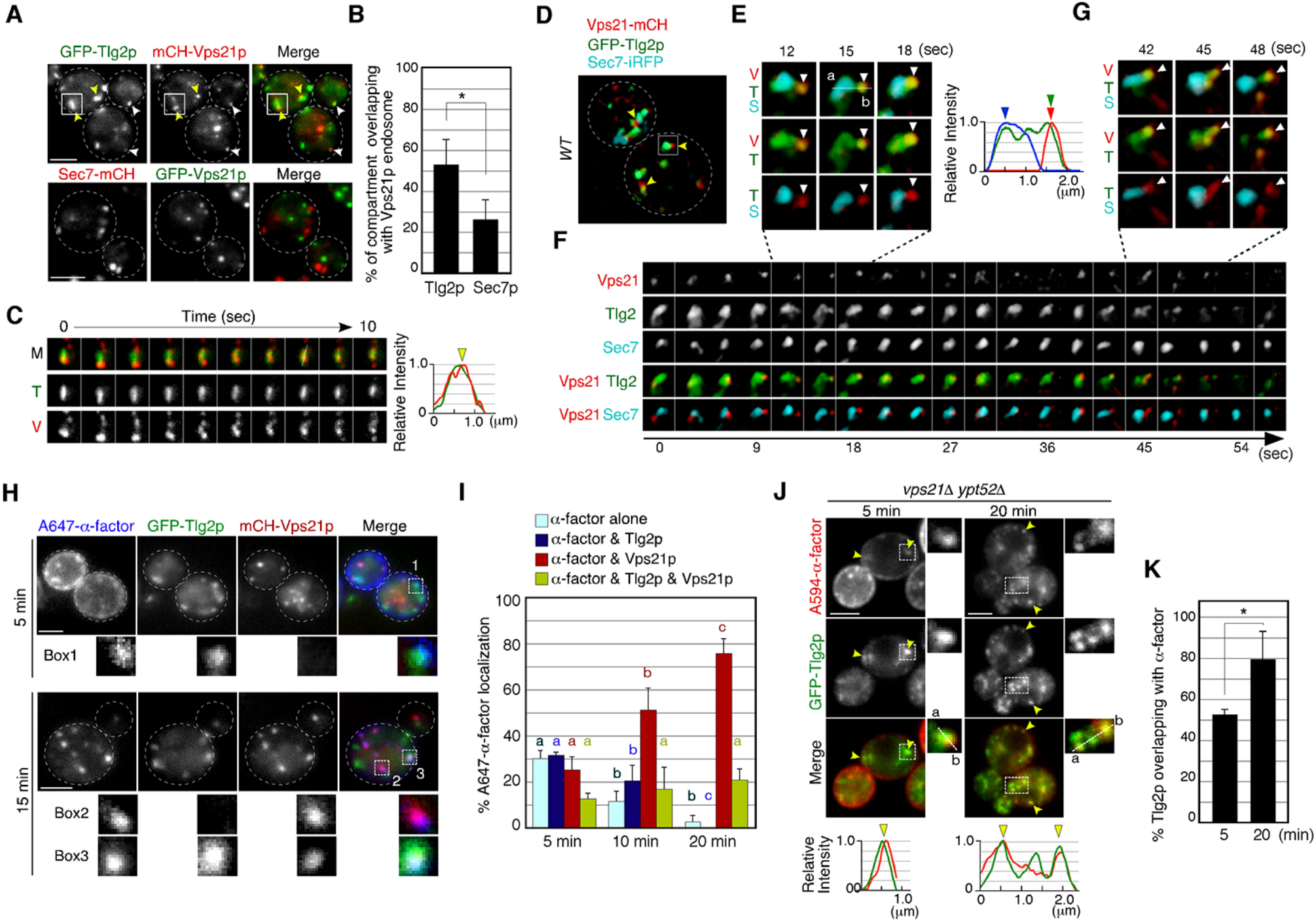

Figure 3. Toshima et al.

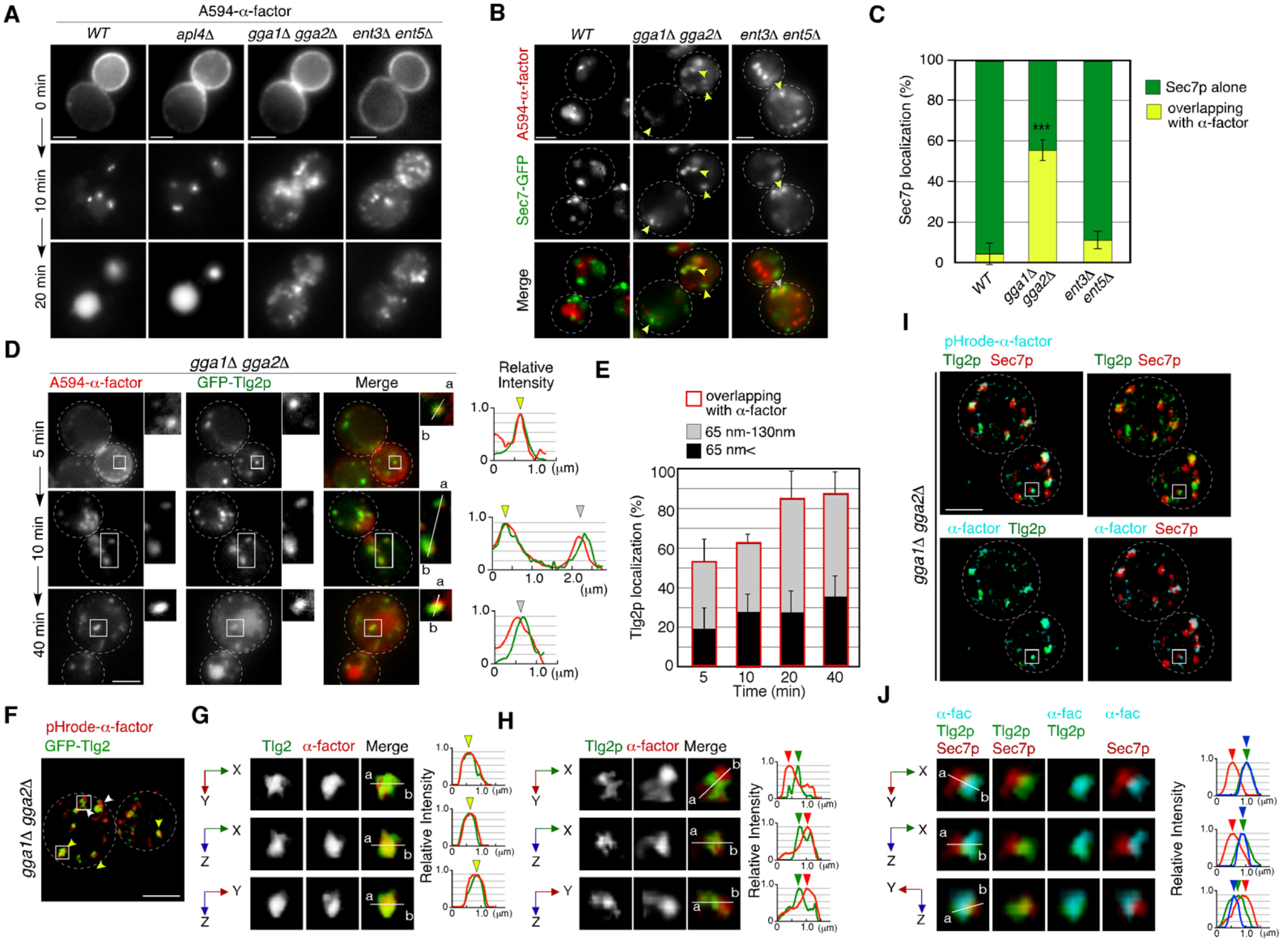

Figure 4. Toshima et al.

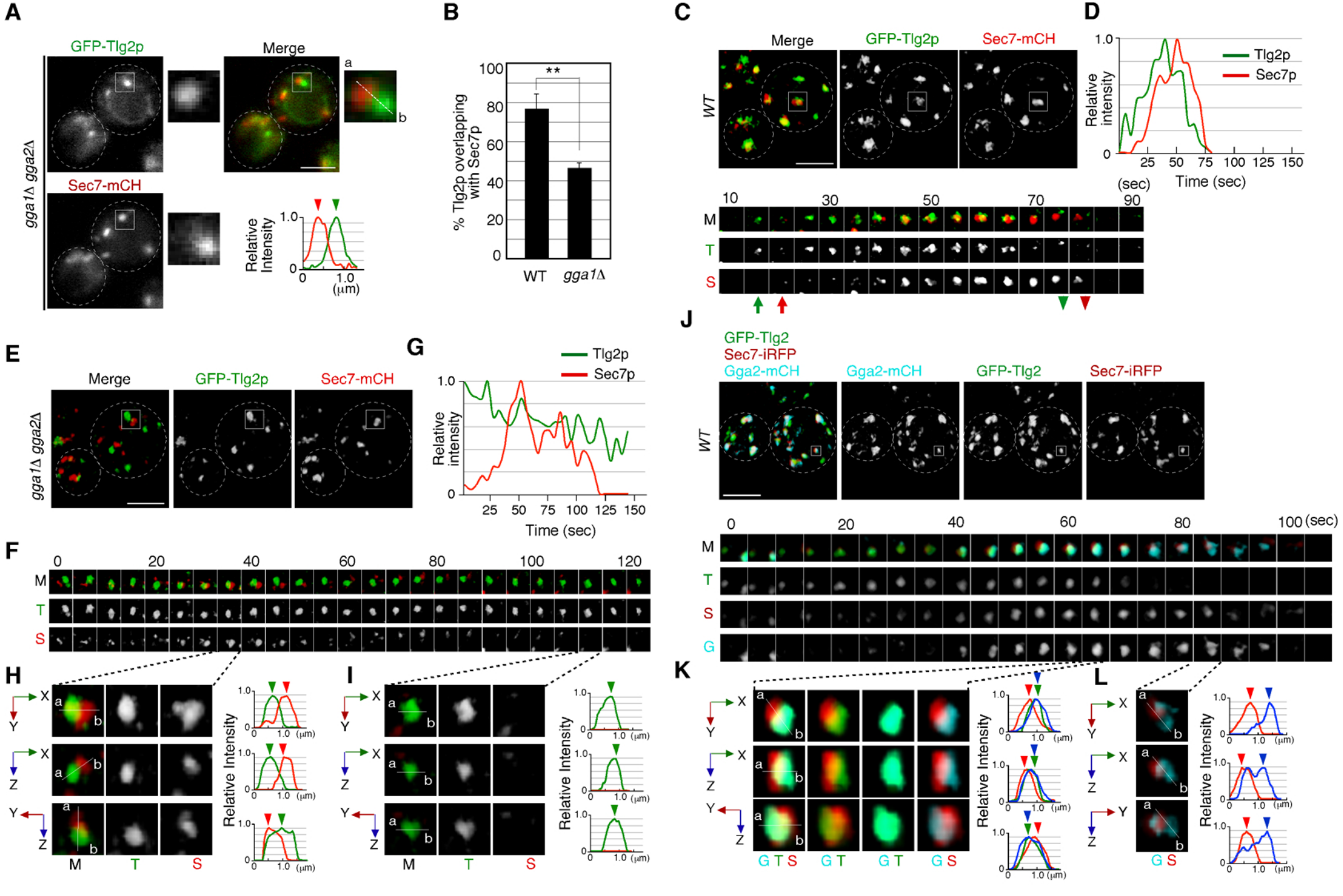

Figure 5. Toshima et al.

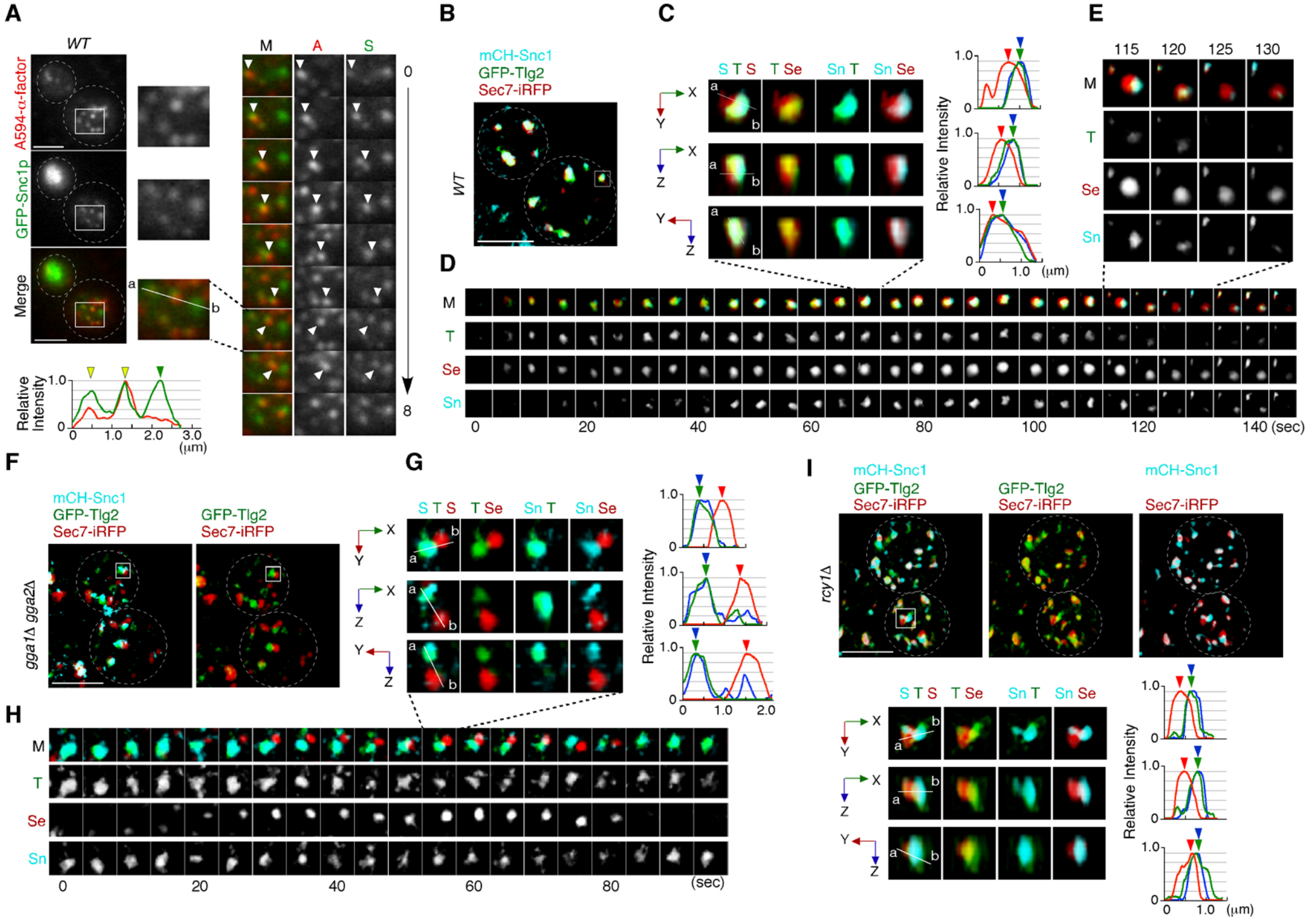

Figure 6. Toshima et al.

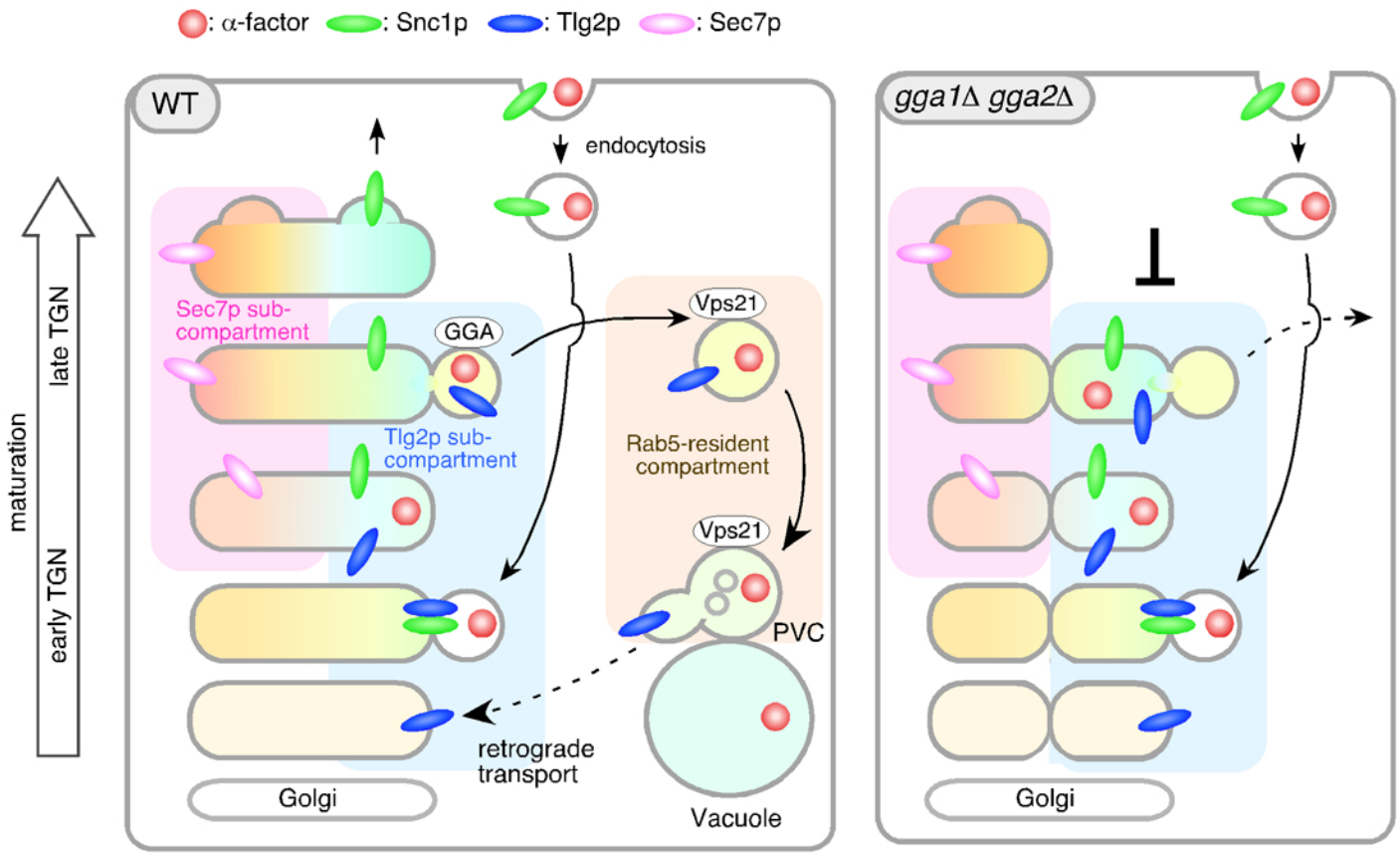

Figure 7. Toshima et al.

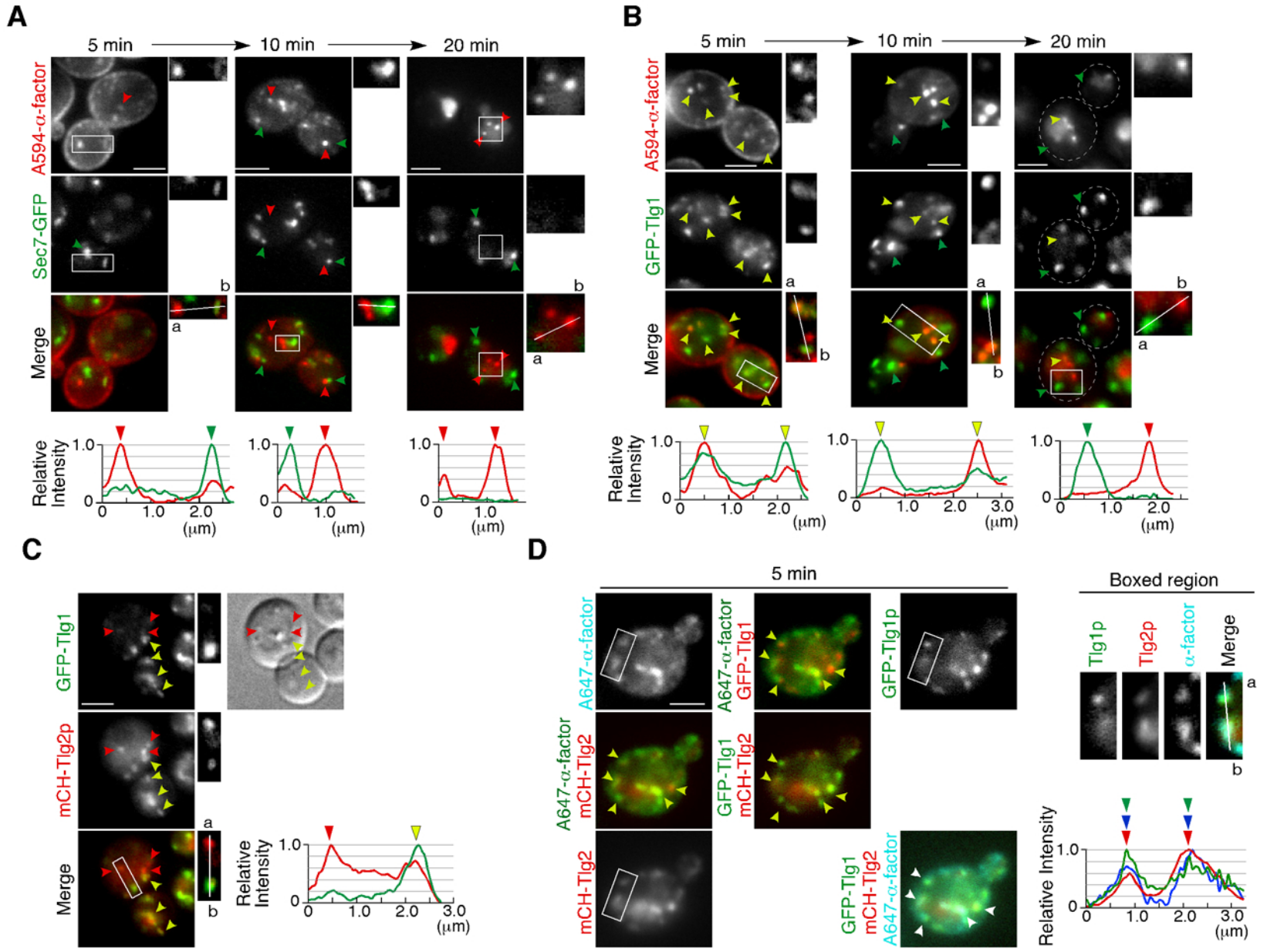

Figure S1. Toshima et al.

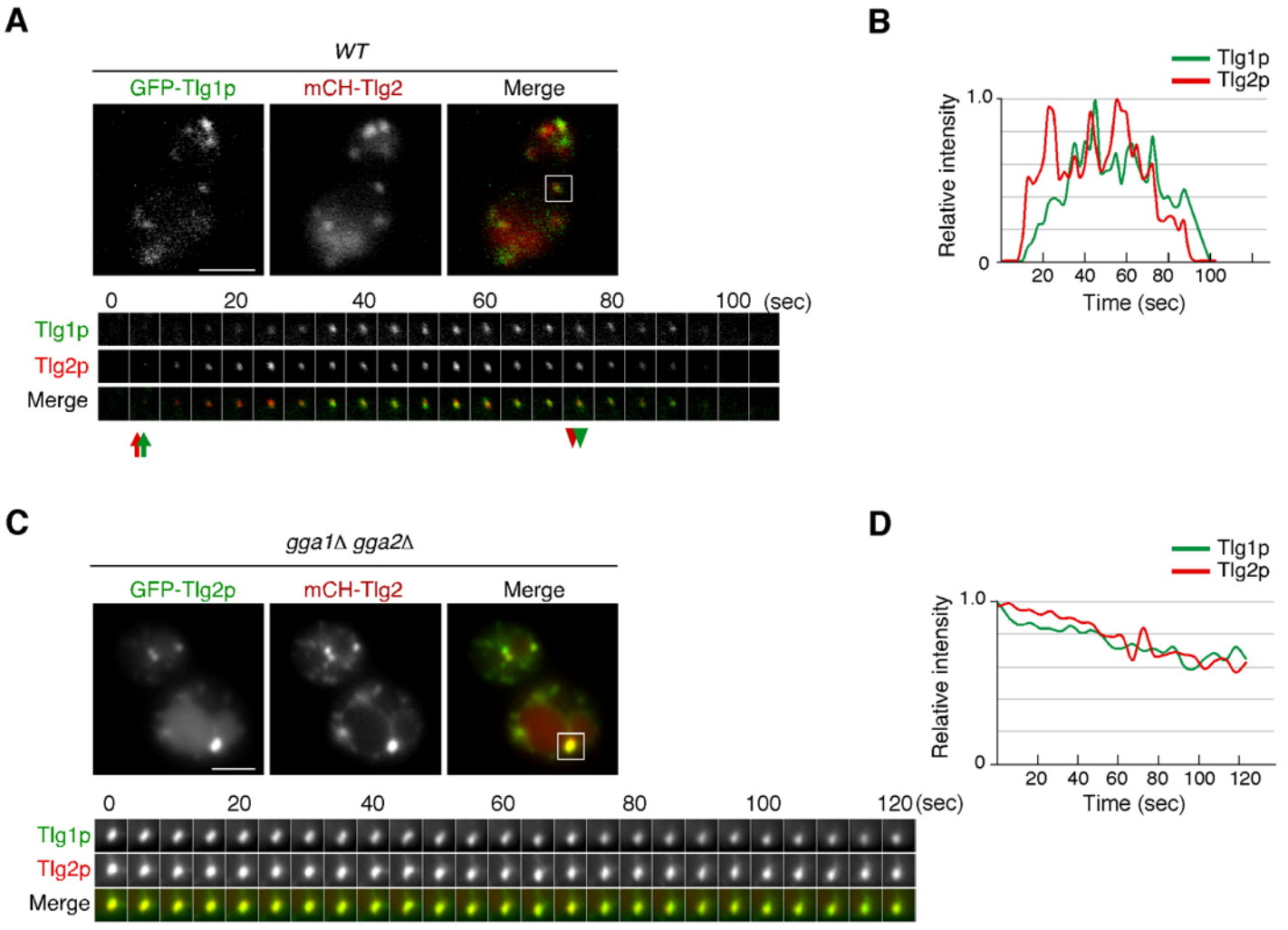

Figure S2. Toshima et al.

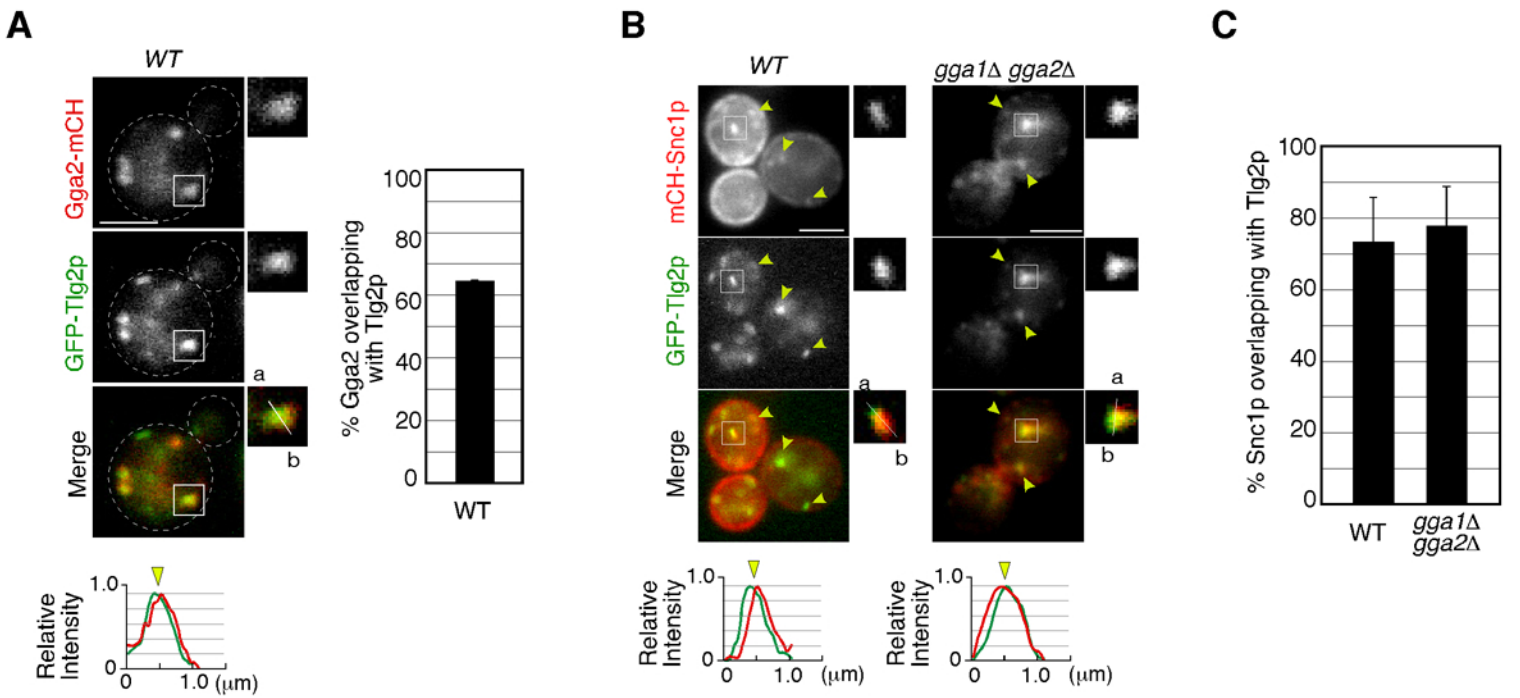

Figure S3. Toshima et al.